Posted on 22 Nov 2022 — The copyright holder is the author/funder. All rights reserved. No reuse without permission. — https://doi.org/10.1002/essoar.10510348.1 — This a preprint and has not been peer reviewed. Data may be preliminary.

Observations of elves and radio wave perturbations by lightning

Maja Tomicic[1], Olivier Chanrion[2], Thomas Farges[3], Janusz Mlynarczyk[4], Ivana Kolmasová[5], Serge Soula[6], Christoph Köhn[7], and Torsten Neubert[8]

[1]DTU Space, Technical University of Denmark
[2]National Space Institute (DTU Space)
[3]CEA
[4]AGH University of Science and Technology
[5]Department of Space Physics, Institute of Atmospheric Physics, Czech Academy of Sciences
[6]Laboratoire d'Aerologie
[7]Technical University of Denmark
[8]Department of Solar System Physics, Denmark

November 22, 2022

Abstract

The electromagnetic and electrostatic fields from powerful lightning heat and ionize the lower ionosphere. The disturbances appear as halos, sprites and elves, and are also observed as perturbations in crossing radio signals. The characteristic of the lightning discharges leading to the various types of perturbations is not fully understood. Here we present an analysis of 63 elves and corresponding VLF and MF signal perturbations from an almost stationary thunderstorm that allows us to untangle some of the dependencies of perturbations on the lightning characteristics. We characterize the perturbations to a VLF-transmitter signal as "long-recovery-early-events" (LOREs), "early" events, or "rapid-onset-rapid-decay" (RORD) events. We find that LOREs are related to high lightning current and bright elves, and their amplitude and sign depend on their location along the signal path. With observations in the ELF and MF band, we find that lightning with elves has three times the impulse charge moment change (iCMC) and ten times the power than lightning of similar peak current without elves. Attenuation in MF links appear in a higher proportion and longer duration observed with elves than with high peak current lightning without elves. The remaining types of VLF perturbations occur without TLEs but with sequences of lightning that produce slowly rising CMCs reaching high values (up to ˜3500 C km within ˜500 ms). Slower rise times lead to lower fields in the mesosphere that may not create significant ionization but instead drive dissociative attachment of free electrons. The depletions can result in perturbations to crossing VLF signals.

Observations of elves and radio wave perturbations by lightning

Maja Tomicic[1], Olivier Chanrion[1], Thomas Farges[2], Janusz Mlynarczyk[3], Ivana Kolmašová[4,5], Serge Soula[6], Christoph Köhn[1], Torsten Neubert[1]

[1]DTU Space, Technical University of Denmark, Lyngby, Denmark
[2]CEA, DAM, DIF, F-91297, Arpajon, France
[3]Institute of Electronics, AGH University of Science and Technology, Krakow, Poland
[4]Department of Space Physics, Institute of Atmospheric Physics, Czech Academy of Sciences, Prague, Czech Republic
[5]Faculty of Mathematics and Physics, Charles University, Prague, Czech Republic
[6]Laboratoire d'Aérologie, Université de Toulouse, UT3, CNRS, IRD, Toulouse, France

Key Points:

- Analysis of 63 elves above a thunderstorm in the Adriatic Sea and perturbations to MF and/or VLF transmitter signals passing the storm
- Lightning causing elves has ∼ten times the power and ∼three times the iCMC of lightning with a similar peak current without elves
- Only LOREs are observed with elves. Shorter VLF perturbations are likely caused by e-field driven electron attachment in the mesosphere

Corresponding author: Maja Tomicic, `majtom@space.dtu.dk`

Abstract

The electromagnetic and electrostatic fields from powerful lightning heat and ionize the lower ionosphere. The disturbances appear as halos, sprites and elves, and are also observed as perturbations in crossing radio signals. The characteristic of the lightning discharges leading to the various types of perturbations is not fully understood. Here we present an analysis of 63 elves and corresponding VLF and MF signal perturbations from an almost stationary thunderstorm that allows us to untangle some of the dependencies of perturbations on the lightning characteristics. We characterize the perturbations to a VLF-transmitter signal as "long-recovery-early-events" (LOREs), "early" events, or "rapid-onset-rapid-decay" (RORD) events. We find that LOREs are related to high lightning current and bright elves, and their amplitude and sign depend on their location along the signal path. With observations in the ELF and MF band, we find that lightning with elves has three times the impulse charge moment change (iCMC) and ten times the power than lightning of similar peak current without elves. Attenuation in MF links appear in a higher proportion and longer duration observed with elves than with high peak current lightning without elves. The remaining types of VLF perturbations occur without TLEs but with sequences of lightning that produce slowly rising CMCs reaching high values (up to ∼3500 C km within ∼500 ms). Slower rise times lead to lower fields in the mesosphere that may not create significant ionization but instead drive dissociative attachment of free electrons. The depletions can result in perturbations to crossing VLF signals.

Plain Language Summary

Powerful lightning can create local disturbances to the atmosphere at around 70-100 km altitude. Such disturbances appear as phenomena known as halos, sprites and elves and can also be observed as changes in phase and amplitude of radio communication signals that pass through the disturbed region. The characteristics of the lightning strokes leading to the various types of perturbations is not fully understood. In this work, we analyse 63 elves and corresponding amplitude changes in radio signals from an almost stationary thunderstorm that allows us to untangle some of the dependencies of perturbations on the lightning characteristics. We find that lightning that produce elves has ten times the power and three times the impulse charge moment change than lightning of similar peak current that did not produce elves. Also we find that elves are associated with the longest types of perturbations (∼ 10 min duration) in the VLF radio signals, whereas the shorter types of perturbations (∼ 1 min duration) occur without optical emission. Our results suggests that these are a result of density changes at 70-85 km altitude caused by electron attachment by slower rising electric fields.

1 Introduction

Elves are rings of optical emissions at the base of the ionosphere (∼80-95 km altitude) that expand rapidly up to ∼700 km diameter during ∼1 ms following a powerful cloud-to-ground (CG) lightning stroke. They are emissions from atmospheric constituents that are excited and ionized by collisions with free electrons heated by the electromagnetic pulse (EMP) radiated by the lightning return current (Fukunishi et al., 1996; Barrington-Leigh & Inan, 1999; van der Velde & Montanyà, 2016). Since their first discovery from the space shuttle orbiters (Boeck et al., 1992), elves have been studied from the ground (e.g., Fukunishi et al., 1996; Blaes et al., 2016; van der Velde & Montanyà, 2016; Kolmašová et al., 2021), from space (e.g., Chen et al., 2008, 2014) and with models (e.g., Inan, Sampson, & Taranenko, 1996; Marshall et al., 2010; Marshall, 2012). The properties of lightning return strokes that control the excitation of elve emissions are still not fully understood because comprehensive data are lacking caused, for instance, by limitations in instrument sensor sensitivities, triggered data selection, and the relatively modest number of optical observations of elves. Whereas the radiated EMP is proportional to the time derivative of the peak current, the most commonly adopted parameter for elve probability is the peak current itself because it is a parameter provided by lightning detection networks. An estimate of the lower limit required to generate elves range from ∼38 kA (Chen et al., 2014), where elves were observed with the ISUAL spectrophotometer from space, to ∼130 kA (van der Velde & Montanyà, 2016) based on camera observations from ground in Spain and France. Observations in the western United States concluded that the threshold for 50% probability of elves was 88 kA and 90% probability at 106 kA (Blaes et al., 2016). Global variations in the height of the ionosphere and electron density gradients with altitude may influence the production of elves, as well as meteorological variations such as thunderstorm altitudes, and thereby the average lightning channel length (Blaes et al., 2016). Thus, van der Velde and Montanyà (2016) found elves far more likely in maritime winter thunderstorms than summer thunderstorms over land and Chen et al. (2014) found only dependence on stroke energy, but no significant oceanic and land difference. The diversity of conditions in the above reports points to the difficulty in determining a globally and seasonally independent lower limit on peak current (or other lightning parameters) for the causative lightning of elves.

Narrow-band navigational transmitter signals in the VLF band propagate in the earth-ionosphere wave-guide. They reflect at altitudes of elves and the signal properties are therefore affected by conductivity changes at this boundary. The electron density changes associated with elves (Marshall et al., 2010) cause steplike perturbations to the transmitter signals (amplitude and phase) if the transmitter-receiver (TR) path crosses the region affected by the elve. Such perturbations are called Long Recovery Early Events (LOREs)(e.g., Haldoupis et al., 2013; Mika et al., 2006; Naitamor et al., 2013; Salut et al., 2012). They fall into the category of "early" VLF events because they are caused by direct coupling of the lightning EMP and the ionosphere, thus showing a very short delay (a few ms) from the return stroke pulse. LOREs persist for tens of minutes, and sometimes the signal does not recover before it is masked by other variations in the signal levels (Mika et al., 2006). The long recovery time is linked to the lifetime of free electrons at this altitude (Rodger, 2003). The LORE phenomenon has almost exclusively been observed in association with elves and is considered the VLF signature of elves (Haldoupis et al., 2013; Mika et al., 2006; Kolmašová et al., 2021), although larger data sets have not been published until now. On the other hand, the physical mechanisms responsible for "early/fast" and "early/slow" VLF events (Inan et al., 1993; Haldoupis et al., 2006), which are similar to LOREs but with recovery within a few minutes, are still under debate (Marshall et al., 2008; Kabirzadeh et al., 2017). They relate to sprites (Inan et al., 1995; Haldoupis et al., 2004, 2010) and sprite halos (Moore et al., 2003); however, numerous observations of early/fast events with no associated transient luminous events (TLEs) also exist (Marshall et al., 2006). To relate to sprites and halos they must be driven by the quasi-electrostatic (QE) field of lightning discharges. The field affects the atmosphere at lower altitudes (70-80 km) where the lifetimes of free electrons are of the order of 10-100 s (Pasko & Inan, 1994; Rodger et al., 1998) in line with the observed recovery rates. Another type of VLF perturbation associated with the QE field of lightning are the so-called "rapid onset rapid decay" (RORD) events (Dowden et al., 1994; Inan, Slingeland, et al., 1996). With onsets within 20 ms and recovery in less that 3 seconds, corresponding to the duration of the field, they are believed to be VLF signatures of the conductivity changes due to heating by QE fields(Inan, Slingeland, et al., 1996).

Narrow-band signals from radio transmitters in the MF band (0.3-3 MHz) reflect during the nighttime at $\sim$105 km altitude and may be absorbed if passing through disturbed regions. Strong CG strokes are found to be associated with ms-duration attenuation of narrow-band radio transmission in a band of 500 - 1600 kHz, with the amplitude of attenuation proportional to the peak current of the causative stroke (Farges et al., 2007). Although MF perturbations are four-five orders of magnitude shorter than VLF perturbations, the size of the perturbed regions is comparable. To understand this brief blackout phenomenon, Farges et al. (2007) modeled the propagation of the MF radio waves through a region of the ionosphere disturbed by the lightning EMP under three different scenarios: that the EMP causes only ionization, only electron heating, and both combined. The results were compared to the absorption calculations obtained in the absence of flashes and showed that electron heating alone could explain the measured attenuation. Moreover, the decay of electron heating, which is less than 100 ms at elve altitudes (Rodger et al., 1998), is the only process that is compatible with the observed attenuation ($1-10$ ms). For comparison, the decay of enhanced ionization is 10,000 times longer. Finally, Farges et al. (2007) concluded that the disturbances could be an additional signature of the presence of elves. However, simultaneous observations of elves and MF blackouts have not been published until now.

In this paper, we present observations of a high number of elves produced over the Adriatic Sea during the night of December 9-10, 2020, with simultaneous observations of perturbations in the signals of one VLF link and seven MF links passing the region. Our goal is to investigate the relationship between lightning characteristics and lightning effects in the ionosphere. For the first time (to our knowledge), optical observations of 63 elves were recorded from an almost stationary storm. The observations offer a rare opportunity to limit the influence of geographic location, local time and season, viewing conditions and instrument sensitivity while still having a large data sample. We include in our analysis impulse current moment changes (iCMC) and charge moment changes (CMC) of selected strokes derived from Extremely Low Frequency (ELF) measurements and energy of causative strokes from broadband electric field measurements. The relationship between the LOREs of positive and negative polarity is discussed from perturbations by a second storm on the Italian south coast towards the Tyrrhenian Sea.

2 Data, instrumentation and methods

2.1 Lightning data

We use lightning data from the Vaisala Global Lightning Dataset, GLD360 (Said et al., 2010; Said & Murphy, 2016). It contains time, location, peak current and type (CG or intracloud (IC)). The detection efficiency (DE) and location accuracy (LA) in the USA is evaluated to $\sim$75–85% relative to the National Lightning Detection Network, which has a flash DE >95% (Mallick et al., 2014). The median LA is 1.8 km. The accuracy in the Adriatic sea is assumed to be the same, as the sensor density is similar to that in the USA (R. Said, personal communication, March 17, 2021).

The vertical broadband electric field from 1 kHz to 5 MHz was measured with a dipole whip antenna installed in the center of France, 900 to 1050 km from the storm location (labelled "BB" in Figure 1) (Farges & Blanc, 2011). The system triggers if the field exceeds 2 V/m, storing 30 ms of data from 6 ms before the trigger at a sampling frequency of 12.5 MHz. We use the measurements to characterize lightning and blackouts of MF radio transmitter signals.

The current moment waveform (CMW) and CMC were obtained from measurements of an ELF receiver system in the Bieszczady mountains in Poland (49.2°N, 22.5°E ∼850 km from the storm and labelled "ELF" in Figure 1). It measures the magnetic field component with two antennas aligned in the north-south and east-west directions in the frequency range 0.02 Hz to 1.1 kHz. The receiver features a Bessel anti-aliasing filter with a bandwidth of 900 Hz. The sampling frequency is 3 kHz. The CMW and the CMC were reconstructed using the method of Mlynarczyk et al. (2015) that accounts for the dependence with the frequency of the signal attenuation and the propagation velocity in the ELF range.

2.2 VLF receiver

A Sudden Ionospheric Disturbances (SID) monitor measures perturbations to narrowband VLF signals from powerful transmitters used for communication with submarines. The monitor used in this study is operated by the Slovak Organization for Space Activities and placed in Bojnice, Slovakia (48.8°N, 18.6 °, labelled "SID" in Figure 1). It can record up to sixteen VLF transmitters simultaneously with a sampling frequency of 2 Hz. We use the NSY transmitter operated by the Naval Computer and Telecommunications Station in Sicily (37.1°N, 14.4°E), which broadcasts at 45.9 kHz with 250 kW. The signal propagates from Sicily to Slovakia (∼1345 km) and reflects multiple times at the surface of the Earth and the bottom of the ionosphere. The propagation great circle path (GCP) of the NSY signal crosses directly the thunderstorm location (see Figure 1).

2.3 Optical observations

The optical observations are performed by a TLE observatory installed in Rustrel, France (43.94° N, 5.48° E) at 1025 m altitude. It is mounted on a building made available by Laboratoire Souterrain à Bas Bruit (LSBB). The camera is a Watec 1/2" monochrome CCD camera (WAT-902H) with a 16 mm lens that gives ∼23° horizontal and 17° vertical field of view (FOV). It takes 50 interlaced fields per second, corresponding to a time resolution of 20 ms. The images are time referenced after synchronization with an NTP server, giving an absolute time uncertainty below 5 ms. The camera is mounted on a Quick-Set motorized Pan-Tilt unit allowing for active and automatic tracking of thunderstorms. The night of the observations, the camera tracked two thunderstorms automatically, selecting a new pointing direction every 15 minutes. The camera, therefore, pointed away from the storm during parts of the night. The analysis excludes strokes that occurred in these gaps. From 02:45 UTC the camera stayed in the same position for the rest of the night.

2.3.1 Methods and error estimations

Figure 2, shows an image of an elve that occurred at 03:57:56.578 UTC on December 10th, 2020. From the images, we estimated their altitude and relative brightness. Following van der Velde and Montanyà (2016), we calculated the altitude by combining the elevation of the elve centers retrieved from the software 'Cartes du ciel' with the location of the CG stroke reported by GLD360, assuming a spherical earth with radius of 6370 km and a camera altitude of 1025 m. Before the image analysis, the background for each elve, determined as the mean value of two interlaced fields preceding the elve, was subtracted. The same fields were used to determine the elevation angle of the FOV. The elves are faint and diffuse, and their centers can be difficult to determine, which introduces an error in the elevation angle. We found that the read-out error was less than

0.1 deg, which corresponds to an altitude uncertainty of ±1.4 km at 800 km distance to the elves. The uncertainty in the location of the parent strokes (median value 1.8 km (Said & Murphy, 2016)) introduces an uncertainty of around 0.3 km at 800 km distance to the storm. We estimated the relative brightness of the elves from the sum of all pixels in the background subtracted elve images after scaling by the size of the elve in the image. The brightest elve was used as a reference.

3 Meteorology and storm development

On December 9, 2020, a low-pressure system was centered over northern Italy according to the geopotential at 500 hPa with a minimum of about 5.275 km (red lines in Figure 1). The counter-clockwise winds reached up to 40 m s^{-1} at 500 hPa (∼5.5 km), corresponding to large geopotential gradients along an arc extending over northern Africa and southern Italy. This jet carried warm, humid air from the Mediterranean Sea into the Adriatic Sea, enhancing strong atmospheric forcing in the region. Over the Adriatic Sea, the wind shear between 1000 and 500 hPa (0-5.5 km) was modest, and the CAPE was moderate ($<$ 700 J kg^{-1}) and higher over water. These conditions led to several electrically active cells that produced lightning with very high peak currents. Figure 3 shows the cloud top temperature (CTT) in the Adriatic Sea where the elves were observed (rectangle in Figure 1). The CTT is obtained from the 10.8 μm band of the Spinning Enhanced Visible and InfraRed Imager (SEVIRI) on the Meteosat Second Generation (MSG) satellite and is shown here for each hour of elve observation (20:00 UTC to 05:00 UTC). The CTT data is corrected for parallax, corresponding to 0.1° in latitude and 0.03° in longitude for cloud tops at ∼10 km altitude. All CG strokes with peak currents above 200 kA absolute value are plotted with black crosses, and the elve-producing strokes are plotted in green. The elve-producing cells are less than 100 km across at CTT<-40°C (blue regions in Figure 3). The coldest CTT is about -60°C, which is not much colder than the tropopause (-56°C) at the same location, suggesting the clouds did not reach much above the tropopause. The elves were caused by strokes over the Adriatic Sea, where CAPE was higher than over land. In the second active region in southern Italy, more CG strokes are over land or at the coastline where CAPE in this region is higher (Figure 1). The CG stroke rate of the Adriatic storm does not exceed 10 CG strokes per minute. The relatively low convective activity, seen from the modest development of clouds cells and low stroke rate, is due to the limited CAPE and wind shear over the Adriatic Sea. From GLD360 we also get that 91% of the CG strokes produced in the Adriatic region (gray rectangle in Figure 1) from 19 to 6 UTC were negative with high average peak currents at -92 kA. The elve-producing strokes all have absolute peak currents stronger than 228 kA with an average of 453 kA.

4 Observations

4.1 Elves

During the night of the storm, the camera at Rustrel detected 63 elves. One is shown in Figure 2, and the rest is in the Figures S1-S63 in the Supporting Information. The lowest altitude at the storm that the camera could observe was 50 km (at 750 km distance) and 80 km (at 950 km distance). Thus, we cannot rule out other TLEs, such as sprites and halos, occurring below these altitudes. The camera observed the storm from 20:00 to 05:35 UTC with gaps totaling one hour and 45 minutes (22:00-22:30; 23:30-00:00; 00:30-01:15 UTC).

The optical characteristics were studied for all but a few elves. In four cases, no parent stroke was reported by GLD360 that allowed the estimation of their distance, three were too faint to define their shape, and the brightness of four could not be determined because the moon was behind the elve in the video field. Out of 63 elves, 56 were used for the brightness and altitude calculation.

The altitudes of the elves ranged from 80-90 km, which is within the range and variability of the results in van der Velde and Montanyà (2016). All elves below 83 km occurred in the first hour of observations. We attribute this to the storm cell that was active during this hour rather than to changes in the ionosphere based on results from the NASA international reference ionosphere model (IRI). There is no clear trend between altitude and local time for the rest of the night. The relative brightness varies down to ∼17% of the brightest elve. The brightness is correlated with the peak current and the Power Spectral Density (PSD) of the parent stroke in the band of the broadband receiver (see below), a parameter discussed in later paragraphs.

4.2 Lightning

During the periods the camera observed the storm, GLD360 detected 234 strokes with absolute values above 200 kA within the camera's FOV, leading to 175 of these that did not produce elves (CG strokes for four elves were not detected). To understand why some produced elves and others not, we made a parameter analysis of the waveform of the vertical electric field from the lightning strokes, measured by the broadband receiver in France. For each stroke, we determined the maximum amplitude of the ground wave (E_{GW}), the rise-time of the electric field pulse, defined as the time from 50% to 90% of E_{GW}, and the fall time from the maximum to the background. These statistics showed no apparent difference, a conclusion also reached when we averaged and compared the complete waveforms of those that generated elves with those that did not (see Figure S64 in the Supporting Information).

In Blaes et al. (2016), the peak current of the CG stroke is found to be a decisive parameter for elve generation, with a probability reaching 50% at 88 kA. Other authors found thresholds from 38 to 130 kA (Chen et al., 2014; van der Velde & Montanyà, 2016). In our case, the formation threshold of elves is around 200 kA. The variability of reported thresholds is likely an effect of the sensitivity of the optical instrument used (camera or photometer, for example), or uncertainty in the estimation of the peak currents reported by the detection networks. However, a question remains why not all high-current strokes generate elves, as noted in Kolmašová et al. (2021).

To explore this question further, we computed the electric field wave power, $P(E^2)$, which is the frequency integral of the electric field PSD over the whole antenna bandwidth (1 kHz to 5 MHz) using the method of Ripoll et al. (2021). It is computed over 1.5 ms from the arrival time of the ground wave, to include the ground wave and all the sky waves. Figure 4 shows that the CG strokes producing elves have about one order of magnitude larger power, and also three orders of magnitude larger power than the typical flashes analyzed in (Ripoll et al., 2021) using the same electric field sensor. This suggests that the generation of elves depends on the complete electromagnetic energy release of the stroke.

We also analyzed ELF measurements of the electromagnetic signals from a subset of the lightning strokes from the sensor in the Bieszczady Mountains in Poland. The selection included high-current strokes with and without elves, and strokes with elves combined with no, weak or strong LOREs. We calculated the current moment (CM), the CMC and the impulse charge moment change (iCMC) (Cummer & Lyons, 2004) defined as the total CMC during the first 2 ms of the lightning stroke according to the method of Mlynarczyk et al. (2015). The iCMC is likely more relevant for elves than the total CMC since elves are generated within the first milliseconds. The results and other relevant stroke parameters are presented in Table 1. We see that the iCMC and the CM are three times larger for strokes that generate elves. Larger values can result from larger currents, longer channel lengths, or both. Since GLD360 data only provide the maximum current obtained in the VLF range, one cannot expect full correlation with the iCMC or CM, as pointed out in Lu et al. (2012). Their relation to LOREs is discussed in a following paragraph.

Table 1. Comparison of impulse charge moment change (iCMC) and current moment (CM) for strokes that produced elves, LOREs (strong or weak as sL or wL, respectively) or not. *reported polarities disagree.

Event	Time (UTC)	Lon (deg)	Lat (deg)	Peak current (kA)	iCMC (C km)	CM (kA km)
E + sL	12-09 20:09:08.217	15.46	43.39	-639	-133.2	-122
E + sL	12-09 22:48:54.353	16.56	42.90	-725	-148.5	-146
E + sL	12-10 01:33:38.668	15.68	43.09	-520	-146.6	-137
E + wL	12-09 23:05:50.076	16.67	42.97	-504	-106.5	-93
E	12-09 23:14:30.984	16.68	42.87	-535	-134.0	-120
E	12-10 01:16:58.561	14.84	42.81	-498	-117.4	-108
No E	12-10 20:25:15.397	15.27	43.34	+359*	-59.1	-55
No E	12-10 01:41:08.681	18.54	42.51	-430	-29.3	-33
No E	12-10 02:33:11.310	18.45	42.66	-378	-32.7	-30
No E	12-10 03:31:06.092	14.74	42.85	-426	-43.8	-39

4.3 VLF transmitter signal perturbations

The amplitude of the NSY VLF signal from the night of December 9-10th is shown in Figure 5 on different temporal scales. The variation on scales larger than ∼30 minutes are not related to thunderstorm activity, but to other ionospheric processes because the signal from the same transmitter during a night without storms shows similar variations. However, amplitude perturbations on shorter scales are multiple, and many correlate in time with lightning activity detected by GLD360. These are identified using the criterion that the perturbation amplitude must be greater than 0.25 dB relative to the average amplitude (in dB) of the preceding 10 seconds. This condition corresponds to a threshold of 4σ, where σ is the average standard deviation for the night. The value is close to the typical value at 0.2 dB of Inan, Slingeland, et al. (1996). In addition, we require that a lightning stroke be detected by GLD360, or an elve by the camera, within 0.5 sec before the perturbation, corresponding to the temporal resolution of the receiver. The algorithm used to identify candidate events is used on a 3-point moving average of the signal, shown in Figure 6c in red. All candidate events are manually validated and categorized. The events are grouped in three categories: LOREs, the so-called ”early/fast” or ”early/slow” events (Inan et al., 1993; Haldoupis et al., 2006), and some events that are also early and fast but only last for 0.5-2 seconds, similar to the previously observed rapid onset, rapid decay (RORD) signatures (Dowden et al., 1994). In Figure 6 we show examples of the three types.

The time resolution of the VLF receiver (0.5 s) is sufficient to classify, with a high probability, events as ”early” and to exclude lightning-induced electron precipitation that has onsets of 0.3-1.6 s relative to their causative stroke (Burgess, 1993; Peter & Inan, 2007). However, it does not allow for classification of the onset duration below 500 ms and therefore ”early/fast” (onset <20 ms) and ”early/slow” fall in the same category, which we call ”early” events (although, by definition LOREs and RORD are also early events). The origin of the ”early/fast” and ”early/slow” events is discussed in a later paragraph.

Based on their duration and shape, it is rather simple to categorize many perturbations as either LORE, ”early” events, or RORD events. RORD events are simple because they only appear as short perturbations of 1-4 measurement points (2 Hz sampling frequency) before the signal returns to pre-lightning conditions. We identify 33 RORD events (3 with negative amplitude and 30 with positive amplitude of perturbation). Note that the algorithm could miss some because the 3-point smoothing puts them below the 0.25 dB threshold. The two other types are identified using a 20-point moving average (corresponding to 10 sec), and are shown in red in Figures 5 and 6a,b. ”Early” events appear as sudden increases in the signal with a recovery (decrease of signal) that starts within 10 seconds of the peak. These events, therefore, appear as a peak with no plateau on the top in the smoothed signal. LOREs are defined as step-like perturbations that can be either positive or negative and that do not show recovery within the first 20 seconds. It means there will be either a plateau after the step or the amplitude keeps decreasing/increasing for at least 20 sec (see the example in Figure 6a). We identify 68 ”early” events (all with positive amplitude) and 18 LOREs (14 negative and 4 positive). The events are marked in Figure 5 and the main characteristics of the lightning strokes related to the three types of perturbations are given in Table 2. There are also signal perturbations related to high peak current lightning or even elves that have the shape of negative amplitude LOREs except that the onset is significantly slower at 1 to 3 s. One example is seen in Figure 5b at 22:46:53 UTC. For brevity, such events are not investigated further in this work.

Because of the considerable variation of the background signal and the high number of lightning-induced perturbations, it is hard to determine a recovery time for the individual perturbations. However, for all the ”early” events, the recovery time looks shorter than 3 minutes (most are ~ 1 min), which is consistent with the typical recovery time of these events. The LOREs may not recover before other variations mask them. However, they appear longer than the ”early” events. In some cases, the perturbation is hard to categorize (positive LORE or ”early” event) because the LORE step or the shape of an ”early” event is unclear due to the varying background signal. Another complication is that perturbations can overlap. Thus, a few events can be miscategorized.

	LORE	”Early”	RORD
# of events (pos/neg amplitude)	18 (4/14)	68 (0/68)	33 (30/3)
Lightning peak current parameters in absolute value			
Range (kA) [min max]	[314 725]	[3 660]	[5 315]
# CG/IC	15/0*	49/19	31/2
# Neg/pos	14/1*	30/38	25/8
Mean/Median (kA)	526/526	82/45	124/107
95 % conf. int. (kA)	[461 592]	[55 108]	[94 154]

Table 2. Statistics from GLD360 data on the three types of VLF perturbations.

*Three events do not have parent lightning detected by GLD360, but coincide with elve.

Figure 7a,c shows the location of the lightning strokes related to the different types of perturbation and the histogram in Figure 7b shows the minimum distance from the stroke to the VLF path for all three types.

4.3.1 LOREs

13 out of 14 negative LOREs were associated with elves caused by lightning strokes of peak current ranging from 314 to 725 kA. The remaining negative LORE (at 23:36 UTC) occurred simultaneously with a lightning stroke with a peak current of +536 kA when the camera was not observing the storm. Thus, it is likely that there was an elve at the time. These results show that the decreases considered as LOREs are related to elves. Nevertheless, the drop in the signal amplitude is counter to most reported LOREs

that exhibit a steep increase in amplitude, believed to be related to a better VLF signal reflection efficiency (Haldoupis et al., 2013; Kolmašová et al., 2021). The four positive LOREs were generated by the storm on the west coast of Italy, not covered by the camera. However, the related lightning strokes had high peak currents, ranging from -383 kA to -631 kA, making them very likely to produce elves. Therefore, we infer that a decrease or increase in the signal amplitudes is a signal propagation effect that depends on the relative locations of the transmitter, disturbance, and receiver, as proposed from observations and models (Haldoupis et al., 2013; Naitamor et al., 2013; Marshall & Inan, 2010). As seen from Figure 5, most of the recorded elves (78%) were not associated with perturbations in the VLF signal, although they were caused by very high peak current lightning and occurred within 150 km from the VLF link. Also, the LOREs have very different amplitude. These observations will be discussed in Section 5.

4.3.2 "Early" VLF events

The "early" events, all seen as increases in the VLF signal, are unrelated to elves but correlate in time with lightning of both polarities within 150 km of the VLF path. The median of the absolute values of peak currents is 45 kA, and as seen from Table 2, this is much lower than for the LORE producing strokes and lower than the strokes related to RORD events. The mean peak current and 95% confidence interval calculated for the "early" event strokes match the peak current intensities reported for this type of phenomenon earlier, e.g., 20 kA to 180 kA in Inan, Sampson, and Taranenko (1996).

We calculate the CMC for the discharges related to three of the "early" events (called a, b and c) and present the results in Table 3 together with the stroke parameters reported by GLD360. Figure 8 shows the current moment waveform and CMC for "early" event c. The three events are chosen because they are related to lightning from the same storm cell. Thus we limit the influence of differences in storm cell characteristics, relative location and local time. The time of the three events is read from Table 3 and the VLF signal perturbations are shown in Figure 5c. As seen from the example in Figure 8, the CM waveform around the time of the event shows a series of discharges and continuing current that make the CMC increase for almost 500 ms. All three "early" events studied here had similar signatures in ELF, and the CMC increased for at least 400 ms in all cases.

Some "early" events (19/68) coincide with IC discharges detected by GLD360 and without accompanying CG strokes. GLD360 reports peak current amplitudes for these IC discharges between 3 and 42 kA. We checked Earth Networks lightning data as well, and for 10 of these events, they also only report IC discharges. At the time of the remaining 9 events, Earth Networks reports either no lightning or a very low peak current (0.3 to 7.5 kA) CG stroke. The locations of the IC discharges are marked with cyan stars in Figure 7c, and as seen here, all of them are located close (within 34 km) to the VLF path. In these cases, the lightning detection system could have missed the causative CG stroke. However, it is unlikely that two independent lightning detection networks both miss CG strokes but detect weak IC pulses. In addition, the similar location of the events suggests that they are, in fact, related to IC processes. Our interpretation aligns with Johnson and Inan (2000), who report on measurements of "early/fat" events without a parent CG but with spheric signatures interpreted as intracloud pulses, and many CG strokes with high currents close to the VLF signal path that were not associated with VLF events. They suggest that "early/fast" VLF events are exclusively produced by lightning episodes that include a large IC cluster. In addition, Haldoupis et al. (2006) note that the IC activity of weaker but densely clustered sferics can explain the slower onset of "early/slow" events that do not match the timescales of return strokes.

Table 3. Comparison of charge moment change (CMC) for discharges at the time of "early" and RORD events. The lightning stroke parameters (GLD360) are only shown for the strongest discharges, although weaker discharges were also detected in most cases. *reported polarities disagree.

Event	Time (UTC)	Lon (deg)	Lat (deg)	Peak current (kA)	CMC (C km)
"Early" event a	23:17:50.311	16.75	42.94	-26	854.1
"Early" event a	23:17:50.616	16.71	42.91	+68	2708.8
"Early" event b	23:29:57.844	16.72	42.87	-210	818.2
"Early" event b	23:29:57.988	16.73	42.90	+19	2876.6
"Early" event c	23:41:10.851	16.76	42.88	+51	3535.2
RORD a	22:53:17.210	16.61	42.96	-229	1374.0
RORD a	22:53:17.679	16.60	43.01	+53	1009.8
RORD b	23:01:25.721	16.67	42.94	-99	1160.5
RORD b	23:01:26.123	16.53	42.85	-39*	547.6
RORD c	23:02:19.6305	16.57	42.92	-33	1176.3

4.3.3 Rapid onset rapid decay events (RORD)

RORD events are believed to be VLF signatures of heating by QE fields in cases where the QE field is insufficient to drive ionization changes (Inan, Slingeland, et al., 1996). Heated electrons cool almost instantaneously, leading RORDs to last as long as the fields, typically less than a few seconds. In the storm, they are linked with lightning of both polarities, with peak currents from 5 to 315 kA. As seen in Table 2, most RORDs (30) were positive amplitude perturbations.

We also calculate the CMC for the discharges that occur at the time of three RORD events (see Table 3 and Figure 5c for the VLF signal). These events are also related to the same storm cell as the "early" events a, b and c. From Table 3 it is clear that the total CMC is smaller for the RORD events than for the "early" events; however, the CMC increased for at least 600 ms in all three cases.

4.4 MF radio wave attenuation

As shown by Farges et al. (2007), the electromagnetic fields generated by lightning may heat electrons of the lower ionosphere causing millisecond-duration reduction of the amplitudes of signals from MF radio stations. To explore the relationship between such perturbations and lightning with and without elves, we identified 7 MF transmitters from www.mwlist.org, where the signals to the receiver pass over the storm. The measurement concept is shown in Figure 9. The top panel shows the broadband spectrogram corresponding to the elve at 03:57:56.578 UTC, the middle panel shows the corresponding narrowband signal amplitudes of four MF stations at 540 kHz, 576 kHz, 630 kHz, and 891 kHz, and the bottom panel shows the GCPs of the signals from the transmitters to the receiver. The attenuation is most pronounced at 540 kHz, smaller for the three other frequencies and absent in the remaining three links. From the map, we see that the four links impacted pass close to the center of the elve.

For the 59 events with lightning and elves, at least one link is impacted in 86% of the cases, in line with the observation of Farges et al. (2007) for flashes over 60 kA. For the MF attenuation related to the 175 CG high-current strokes that did not produce elves, we found that 53% of the events had at least one attenuated link. The numbers are given in Table 4.

The same technique used by Farges et al. (2007) was systematically employed here to calculate the temporal variation of the attenuation amplitude. The peak attenuation, onset time, rise time and duration of the events were estimated for the seven MF radio links. The averaged values of links with perturbations are shown in Table 4 for the 59 events with elves and the 175 without. The mean peak attenuation is stronger than found by Farges et al. (2007), however they showed that the peak attenuation increases with the peak current. The found value is coherent to the ones calculated for CG strokes with peak current higher than 125 kA. The onset and rise time mean values are like those of Farges et al. (2007), whereas the duration is shorter, particularly for strong CGs strokes that are 5-8 ms in Farges et al. (2007). Our MF measurements confirm that the phenomenon discussed by Farges et al. (2007) is also present when storms are further from the receiver. Regarding cases with and without elves, no difference can be seen for the amplitude but the rise time and durations are significantly shorter for the latter. This could suggest that the MF perturbations in case of no elves observations are due to short or dim elves not able to trigger the camera. We have indeed cases in absence of elves with P(E^2) which are of the same order of magnitude as with elves.

	MF blackout	Peak att (dB)	Onset time (ms)	Rise time (ms)	Duration (ms)
Elve	86%	-16.30	1.01	1.20	3.44
No Elve	53%	-15.68	1.06	1.00	2.89

Table 4. Mean values for MF perturbations for lightning with and without elves.

5 Discussion

The only types of radio wave perturbations that are observed simultaneously with elves are the LOREs and the MF blackouts. We first discuss how they are related to elves, then continue with "early" VLF events and RORD events.

5.1 Elves, LOREs and MF blackouts

Our observations support the understanding that elves are associated with LORES (Haldoupis et al., 2013), while the early VLF perturbations and RORD events are distinct from LOREs and have other origins. However, the observations also raise questions regarding the relationship between elves and LOREs. First of all, why did 78% of the elves occur without LOREs? Second, why do the LOREs vary in amplitude from 0.25 dB to >1 dB? In the following, we try to answer what determines the generation and amplitude of a LORE.

The five strongest LOREs (at 20:09, 22:48, 01:33, 02:19, and 3:56 UTC) have amplitude decreases close to, or larger than, 1 dB. We refer to them as sLOREs (strong) and the rest as wLORE (weak). As seen from Table 1, the presence or amplitude of LOREs is not mirrored in the parameters derived from the ELF data. For instance, the current moment was smaller for cases with weak or absent LOREs, but not significantly so. We cannot, then, search for an explanation in the ELF data. Turning to the VLF data, Marshall and Inan (2010) present a finite difference, frequency domain model of narrow-band VLF transmitter signal propagation in the Earth-ionosphere wave-guide. They place an electron density perturbation at the ionospheric boundary at 85 km somewhere along the propagation path and calculate the changes in the signal properties at a receiver. They show that the amplitude perturbation can be both positive and negative, that it is most perturbed if the disturbance is where the amplitude at the ground is low, such as an interference null, and can be suppressed entirely if it falls at an interference null at the reflection altitude. The amplitude also depends on parameters such as the path length, ionospheric and ground properties, and the signal frequency, however, the night-time electron density fluctuations have a minor influence. In line with their model, we find both positive and negative perturbations in the amplitude and no dependence in local time of the occurrence of LOREs and their amplitudes.

In Figure 7a, we show the location given by GLD360 of the CG strokes that produced elves and LOREs (also "early" and RORD events), and panel c is a zoom of a region close to the VLF path. As noted earlier, Figure 7a shows that the location of all negative LOREs is similar but remarkably different for the positive LOREs. However, the strong LOREs (light blue squares in Figure 7c) are not found closer or at a different geometry relative to the VLF path than the weak LOREs (dark blue diamonds in Figure 7c). Likewise, although many of the elves without LOREs are at a greater distance and different location relative to the VLF signal path, such as those of the cell at $\sim$42.8°N, $\sim$14.5°E, some are very close (see Figure 7c). The observations confirm the model results of Marshall and Inan (2010) and observations in Naitamor et al. (2013) that the relative location of the lightning/disturbance and the VLF path is important for the amplitude and sign of LOREs. It may not be the whole story, though, because we also see from Figure 10a that elves with LOREs are brighter and produced by strokes of higher power, $P(E^2)$, and that the strong LOREs are among the highest in this group. This observation implies that the stroke energy should be large enough to create appreciable ionization before we can observe a LORE. From Figure 10b, we see that the altitude could also be relevant since all elves associated with LOREs were above 86 km. The altitude limit suggested by our results could be related to the reflection height of the VLF signal, which according to Ratcliffe (1959, Figure 12.1) is $\sim$86 km for this particular frequency of 45.9 kHz.

We next turn to the MF blackouts. Since both LOREs and MF blackouts are related to elves, although linked to different processes in the elve generation (ionization and heating, respectively), we looked in our data for a relationship between the two types of phenomena. Figure 10a, b, show that the elves without MF blackouts were caused by lightning with power from 22-56 $(V/m)^2$. However, many elves in this range were also found with MF blackouts. Thus, we cannot determine a threshold. The data in Figure 10b could suggest that elves at lower altitudes are more likely to be related to MF blackouts, however, such a conclusion would be uncertain. It is also uncertain if the location of the disturbance relative to the signal path plays a role. In the region shown in Figure 7c, all but one elve created MF blackouts, which is the same proportion as overall. Understanding the relationship between elves, LOREs and MF blackouts appear to require extensive modeling in addition to data analysis. We can, however, state that MF blackouts may occur without LOREs, but not LOREs without MF blackouts. According to current theories for the two types of perturbations, this statement corresponds to the presence of heating without ionization but not ionization without heating.

5.2 "Early" and RORD events

We can now discuss the origin of the other types of perturbation. The physical mechanisms responsible for early VLF events are still under debate. The candidate mechanisms that have gained the most attention are that they are a result of scattering from ionization regions associated with sprites and/or halos (Haldoupis et al., 2004; Moore et al., 2003). Although the camera horizon was below 70 km for 74% of the "early" events, we do not see optical signatures of sprites or halos. Therefore, we suggest that the "early" VLF events were caused by density changes in the mesosphere that did not produce optical emission.

Marshall et al. (2008) showed that density changes in the lower ionosphere by electron losses through dissociative attachment to molecular oxygen can create measurable amplitude changes in VLF transmitter signals that travel through the disturbed region. The energy required for attachment (3.7 eV) is lower than that of N_2 optical emissions often seen in sprites and elves (7.5 eV) and N_2 and O_2 ionization (15.6 eV)(Haldoupis et al., 2006; Neubert & Chanrion, 2013). This implies that attachment can occur without optical emission and ionization, explaining why we and other studies (e.g., Marshall et al., 2006) report "early" events without associated optical emissions, and also why optical emissions without "early" events are rare (Haldoupis et al., 2004, 2010). The timescale of attachment at ~70 km altitude with high electric fields, but below the threshold field for discharges, is around 0.1 ms while the timescales for screening out the field (the dielectric relaxation time τ_σ) is around 10 ms (Neubert & Chanrion, 2013). This means that electric fields may last long enough for attachment to change the density and thereby the conductivity of the bottom ionosphere introducing perturbations in VLF signals. The timescales of recovery for density changes in the lower ionosphere controlled by attachment-detachment processes is in the order of 100 s (Pasko & Inan, 1994), consistent with the recovery times of the "early" events. As discussed in (Marshall et al., 2008), a consequence of this hypothesis is that "early" VLF events caused by attachment-depleted regions would mostly have positive perturbation amplitudes due to less VLF signal absorption in the reduced density region. This scenario is consistent with our results as well as results from other previous studies (e.g., Inan et al., 1993; Inan, Sampson, & Taranenko, 1996; Marshall et al., 2006; Haldoupis et al., 2004).

Marshall et al. (2008) attribute the attachment process to the EMP from successive in-cloud lightning discharges. Because we observe very high CMC related to the early events (Table 3), we suggest that the QE field caused by the CMC related to the discharges could also contribute to attachment, either alone or in combination with the EMP. The CMC appears high enough to produce ionization in the mesosphere. Common threshold values for breakdown in the lower ionosphere are about 600 C km (Cummer & Lyons, 2005), and for winter thunderstorms, sprite producing strokes were found to have average CMC values of 1400 ± 600 C km, with only extreme events exceeding 3500 C km (Yair et al., 2009). However, we know from Pasko et al. (1997) and it is demonstrated and generalized in Hiraki and Fukunishi (2006), that the electric field in the mesosphere depends on the CMC but also on the the timescale of charge removal. Sprites and halos usually occur after an impulsive enhancement of the CMC by lightning flash or current in the continuing discharge in the order of milliseconds. From Figure 8, we see that the events are related to long (~ 500 ms) sequences of discharges, with both larger and smaller discharges some of which are slower than typically and probably related to IC activity. The CMC increases during 10-100 ms, which is likely too slow to produce TLEs. It could, however, be sufficient to increase attachment (Neubert & Chanrion, 2013) that would lower the electron density and perturb the VLF transmitter signal that passes through the affected region.

The short-duration RORD events in which the entire signal amplitude change lasts only for 0.5-2 seconds are consistent with the heating of the ambient electrons by QE fields in cases when heating is not intense enough to exceed the attachment (3.7 eV) or ionization thresholds (15.6 eV). According to this hypothesis, RORD events are equivalent to the MF blackouts. The conductivity changes due to heating alone last only as long as the fields, which is typically a few seconds for QE fields (Inan, Slingeland, et al., 1996) and only ms for the EMP (Farges et al., 2007). When heating energy exceeds attachment or ionization thresholds, the electron density is reduced or enhanced respectively, in which case the medium would relax back to the ambient conditions in the time scales of the local chemistry (typically 10-100 seconds at sprite altitudes (Pasko & Inan, 1994; Rodger et al., 1998)), as is the case in "early" events. The CMCs associated to the four RORD events in Table 3 are clearly smaller than for the early events while their time constants are the same, supporting this theory.

6 Summary

We analyze for the first time observations of a large number of elves (63) from a single storm over the Adriatic Sea and associated perturbations to MF and VLF transmitter signals. We find three types of perturbations in the VLF transmitter signal: LOREs, "early" and RORD events. We also analyze the iCMC and CMC of selected lightning strokes. Based on the observations, we conclude that:

1. Elves are either accompanied by LOREs (14) or no perturbation (49). Thus, elves are not observed with other types of perturbations in the VLF transmitter signal.
2. Our results suggest that bright elves at higher altitudes (>86 km) generated by high energy strokes are primarily associated with LOREs.
3. The sign of the LORE amplitude perturbation depends on the location of the disturbance (elve) relative to the VLF TR path.
4. MF blackouts occur more often with elves (86 %) than with CG strokes of similar high current, but without elves (53 %).
5. CG strokes that produce elves have one order of magnitude higher power $P(E^2)$ and three times higher iCMC than strokes of similar peak current that do not produce elves.
6. "Early" and RORD events correlate with lightning sequences with slowly increasing CMCs (400 ms) that reach high values. The CMC is higher for early events (>3535 C km) than for RORD events (>1176 C km).
7. Both early and RORD events are, in some cases, observed exclusively with IC discharges.

Acknowledgments

This study was made with the use of NSY transmitter data provided by R. Slošiar from the SOSA (Slovak Organization for Space Activities), Bratislava, Slovakia, and for this we are grateful. The authors thank Laboratoire Souterrain à Bas Bruit (LSBB), Rustrel, France, and its staff, for hosting our camera system. We also thank Vaisala and Ryan Said for providing GLD360 lightning data. And Jeff Lapiere and Earth Networks for lightning activity data and useful discussions. In addition we thank Martin Füllerkrug for interesting discussions on lightning waveforms. The authors thank the French AERIS/ICARE Data and Services Center which provided MSG/SEVIRI data for cloud top temperature. They thank the European Copernicus/ECMWF Data Center, for providing ERA5 meteorological reanalysis. The work of IK was supported by the GACR grant 20-0967S. J. Mlynarczyk acknowledges support of the National Science Centre, Poland, under grant 2015/19/B/ ST10/01055.

Data availability

The data used for this publication can be obtained from the public repository (xxx will be available by acceptance xxx).

References

Barrington-Leigh, C. P., & Inan, U. S. (1999). Elves triggered by positive and negative lightning discharges. *Geophysical Research Letters*, *26*(6), 683–686. doi: 10.1029/1999GL900059

Blaes, P. R., Marshall, R. A., & Inan, U. S. (2016). Global occurrence rate of elves and ionospheric heating due to cloud-to-ground lightning. *Journal of Geophysical Research A: Space Physics*, *121*(1), 699–712. doi: 10.1002/2015JA021916

Boeck, W. L., Vaughan, O. H., Blakeslee, R., Vonnegut, B., & Brook, M. (1992). Lightning induced brightening in the airglow layer. *Geophysical Research*

Letters, *19*(2), 99–102. doi: 10.1029/91GL03168
Burgess, W. C. (1993). The Role of Ducted Whistlers in the Precipitation Loss and Equilibrium Flux. , *98*.
Chen, A. B., Kuo, C.-L., Lee, Y.-J., Su, H.-T., Hsu, R.-R., Chern, J.-L., ... Lee, L.-C. (2008). Global distributions and occurrence rates of transient luminous events. *Journal of Geophysical Research: Space Physics*, *113*(A8). doi: 10.1029/2008JA013101
Chen, A. B., Su, H.-T., & Hsu, R.-R. (2014). Energetics and geographic distribution of elve-producing discharges. *JGR Space physics*, *119*, 1–24. doi: 10.1002/2013JA019470
Cummer, S. A., & Lyons, W. A. (2004). Lightning charge moment changes in U.S. High Plains thunderstorms. *Geophysical Research Letters*, *31*(5). doi: 10.1029/2003GL019043
Cummer, S. A., & Lyons, W. A. (2005). Implications of lightning charge moment changes for sprite initiation. *Journal of Geophysical Research: Space Physics*, *110*(A4), 1–9. doi: 10.1029/2004JA010812
Dowden, R. L., Adams, C. D., Brundell, J. B., & Dowden, P. E. (1994). Rapid onset, rapid decay (RORD), phase and amplitude perturbations of VLF subionospheric transmissions. *Journal of Atmospheric and Terrestrial Physics*, *56*(11), 1513–1527. doi: 10.1016/0021-9169(94)90118-X
Farges, T., & Blanc, E. (2011). Champs électriques induits par les éclairs et les événements lumineux transitoires et leur effet sur l'ionosphère. *Comptes Rendus Physique*, *12*(2), 171–179. doi: 10.1016/j.crhy.2011.01.013
Farges, T., Blanc, E., & Tanguy, M. (2007). Experimental evidence of D region heating by lightning-induced electromagnetic pulses on MF radio links. *J. Geophys. Res*, *112*, 10302. doi: 10.1029/2007JA012285
Fukunishi, H., Takahashi, Y., & Sakanoi, K. (1996). Elves: Lightning-induced transient luminous events in the lower ionosphere. , *23*(16), 2157–2160.
Haldoupis, C., Amvrosiadi, N., Cotts, B. R. T., van der Velde, O. A., Chanrion, O., & Neubert, T. (2010). More evidence for a one-to-one correlation between Sprites and Early VLF perturbations . *Journal of Geophysical Research: Space Physics*, *115*(A7), 1–11. doi: 10.1029/2009ja015165
Haldoupis, C., Cohen, M., Arnone, E., Cotts, B., & Dietrich, S. (2013). The VLF fingerprint of elves: Step-like and long-recovery early VLF perturbations caused by powerful ±cG lightning em pulses. *Journal of Geophysical Research: Space Physics*, *118*(8), 5392–5402. doi: 10.1002/jgra.50489
Haldoupis, C., Neubert, T., Inan, U. S., Mika, A., Allin, T. H., & Marshall, R. A. (2004). Subionospheric early VLF signal perturbations observed in one-to-one association with sprites. *Journal of Geophysical Research: Space Physics*, *109*(A10), 10303. doi: 10.1029/2004JA010651
Haldoupis, C., Steiner, R. J., Mika, , Shalimov, S., Marshall, R. A., Inan, U. S., ... Neubert, T. (2006). "Early/slow" events: A new category of VLF perturbations observed in relation with sprites. *Journal of Geophysical Research: Space Physics*, *111*(A11). doi: 10.1029/2006JA011960
Hiraki, Y., & Fukunishi, H. (2006). Theoretical criterion of charge moment change by lightning for initiation of sprites. *Journal of Geophysical Research: Space Physics*, *111*(11), 1–6. doi: 10.1029/2006JA011729
Inan, U. S., Bell, T. F., Pasko, V. P., Sentman, D. D., Wescott, E. M., & Lyons, W. A. (1995). VLF signatures of ionospheric disturbances associated with sprites. *Geophysical Research Letters*, *22*(24), 3461–3464. doi: 10.1029/95GL03507
Inan, U. S., Rodriguez, J. V., & Idone, V. P. (1993). VLF signatures of lightning-induced heating and ionization of the nighttime D-region. *Geophysical Research Letters*, *20*(21), 2355–2358. doi: 10.1029/93GL02620
Inan, U. S., Sampson, W. A., & Taranenko, Y. N. (1996). Space-time structure of

optical flashes and ionization changes produced by lightning-EMP. *Geophysical Research Letters*, *23*(2), 133–136. doi: 10.1029/95GL03816

Inan, U. S., Slingeland, A., Pasko, V. P., & Rodriguez, J. V. (1996). VLF and LF signatures of mesospheric/lower ionospheric response to lightning discharges. *Journal of Geophysical Research: Space Physics*, *101*(A3), 5219–5238. doi: 10.1029/95ja03514

Johnson, M. P., & Inan, U. S. (2000). Sferic Clusters Associated with Early / Fast VLF Events Early / Fast Event Association with. *Geophysical Research Letters*, *27*(9), 1391–1394.

Kabirzadeh, R., Marshall, R. A., & Inan, U. S. (2017). Early/fast VLF events produced by the quiescent heating of the lower ionosphere by thunderstorms. *Journal of Geophysical Research: Atmospheres*, *122*(12), 6217–6230. doi: 10.1002/2017JD026528

Kolmašová, I., Santolík, O., Kašpar, P., Popek, M., Pizzuti, A., Spurný, P., ... Slošiar, R. (2021). First Observations of Elves and Their Causative Very Strong Lightning Discharges in an Unusual Small-Scale Continental Spring-Time Thunderstorm. *Journal of Geophysical Research: Atmospheres*, *126*(1), 1–23. doi: 10.1029/2020JD032825

Lu, G., Cummer, S. A., Blakeslee, R. J., Weiss, S., & Beasley, W. H. (2012). Lightning morphology and impulse charge moment change of high peak current negative strokes. *Journal of Geophysical Research Atmospheres*, *117*(4), 1–16. doi: 10.1029/2011JD016890

Mallick, S., Rakov, V. A., Hill, J. D., Ngin, T., Gamerota, W. R., Pilkey, J. T., ... Nag, A. (2014). Performance characteristics of the NLDN for return strokes and pulses superimposed on steady currents, based on rocket-triggered lightning data acquired. *Journal of Geophysical Research: Atmospheres*, *119*, 3825–3856. doi: 10.1002/2013JD021401

Marshall, R. A. (2012). An improved model of the lightning electromagnetic field interaction with the D-region ionosphere. *Journal of Geophysical Research: Space Physics*, *117*(3), 1–15. doi: 10.1029/2011JA017408

Marshall, R. A., & Inan, U. S. (2010). Two-dimensional frequency domain modeling of lightning EMP-induced perturbations to VLF transmitter signals. *Journal of Geophysical Research: Space Physics*, *115*(A6), 0–29. doi: 10.1029/2009JA014761

Marshall, R. A., Inan, U. S., & Chevalier, T. W. (2008, 11). Early VLF perturbations caused by lightning EMP-driven dissociative attachment. *Geophysical Research Letters*, *35*(21). doi: 10.1029/2008GL035358

Marshall, R. A., Inan, U. S., & Glukhov, V. S. (2010). Elves and associated electron density changes due to cloud-to-ground and in-cloud lightning discharges. *J. Geophys. Res*, *115*, 0–17. doi: 10.1029/2009JA014469

Marshall, R. A., Inan, U. S., & Lyons, W. A. (2006). On the association of early/fast very low frequency perturbations with sprites and rare examples of VLF backscatter. *Journal of Geophysical Research: Atmospheres*, *111*, 19108. doi: 10.1029/2006JD007219

Mika, A., Haldoupis, C., Neubert, T., Su, H. T., Hsu, R. R., Steiner, R. J., & Marshall, R. A. (2006). Early VLF perturbations observed in association with elves. *Annales Geophysicae*, *24*(8), 2179–2189. doi: 10.5194/angeo-24-2179-2006

Mlynarczyk, J., Bór, J., Kulak, A., Popek, M., & Kubisz, J. (2015). An unusual sequence of sprites followed by a secondary TLE: An analysis of ELF radio measurements and optical observations. *Journal of Geophysical Research: Space Physics*, *120*, 2241–2254. doi: 10.1002/2014JA020780

Moore, R. C., Barrington-Leigh, C. P., Inan, U. S., & Bell, T. F. (2003, 10). Early/fast VLF events produced by electron density changes associated with sprite halos. *Journal of Geophysical Research: Space Physics*, *108*. doi:

10.1029/2002JA009816

Naitamor, S., Cohen, M. B., Cotts, B. R., Ghalila, H., Alabdoadaim, M. A., & Graf, K. (2013). Characteristics of long recovery early VLF events observed by the North African AWESOME Network. *Journal of Geophysical Research: Space Physics*, *118*(8), 5215–5222. doi: 10.1002/jgra.50448

Neubert, T., & Chanrion, O. (2013). On the electric breakdown field of the mesosphere and the influence of electron detachment. *Geophysical Research Letters*, *40*(10), 2373–2377. doi: 10.1002/grl.50433

Pasko, V. P., & Inan, U. S. (1994). Recovery signatures of lightning-associated VLF perturbations as a measure of the lower ionosphere. *JGR Space physics*. doi: https://doi.org/10.1029/94JA01378

Pasko, V. P., Inan, U. S., Bell, T. F., & Taranenko, Y. N. (1997). Sprites produced by quasi-electrostatic heating and ionization in the lower ionosphere. *Journal of Geophysical Research: Space Physics*, *102*(A3), 4529–4561. doi: 10.1029/96JA03528

Peter, W. B., & Inan, U. S. (2007). A quantitative comparison of lightning-induced electron precipitation and VLF signal perturbations. *Journal of Geophysical Research: Space Physics*, *112*(12), 1–20. doi: 10.1029/2006JA012165

Ripoll, J.-F., Farges, T., Malaspina, D. M., Cunningham, G. S., Lay, E. H., Hospodarsky, G. B., … Pédeboy, . S. (2021). Electromagnetic power of lightning superbolts from Earth to space. *Nature communications*. doi: 10.1038/s41467-021-23740-6

Rodger, C. J. (2003). Subionospheric VLF perturbations associated with lightning discharges. *Journal of Atmospheric and Solar-Terrestrial Physics*, *65*(5), 591–606. doi: 10.1016/S1364-6826(02)00325-5

Rodger, C. J., Molchanov, O. A., & Thomson, N. R. (1998, 4). Relaxation of transient ionization in the lower ionosphere. *Journal of Geophysical Research: Space Physics*, *103*(A4), 6969–6975. doi: 10.1029/98JA00016

Said, R. K., Inan, U. S., & Cummins, K. L. (2010). Long-range lightning geolocation using a VLF radio atmospheric waveform bank. *Journal of Geophysical Research Atmospheres*, *115*(23), 1–19. doi: 10.1029/2010JD013863

Said, R. K., & Murphy, M. J. (2016). GLD360 Upgrade: Performance Analysis and Applications. In *24th international lightning detection conference.*

Salut, M. M., Abdullah, M., Graf, K. L., Cohen, M. B., Cotts, B. R., & Kumar, S. (2012). Long recovery VLF perturbations associated with lightning discharges. *Journal of Geophysical Research: Space Physics*, *117*(8), 1–6. doi: 10.1029/2012JA017567

van der Velde, O. A., & Montanyà, J. (2016). Statistics and variability of the altitude of elves. *Geophysical Research Letters*, *43*(10), 5467–5474. doi: 10.1002/2016GL068719

Yair, Y., Price, C., Ganot, M., Greenberg, E., Yaniv, R., Ziv, B., … Sátori, G. (2009). Optical observations of transient luminous events associated with winter thunderstorms near the coast of Israel. *Atmospheric Research*, *91*(2-4), 529–537. doi: 10.1016/j.atmosres.2008.06.018

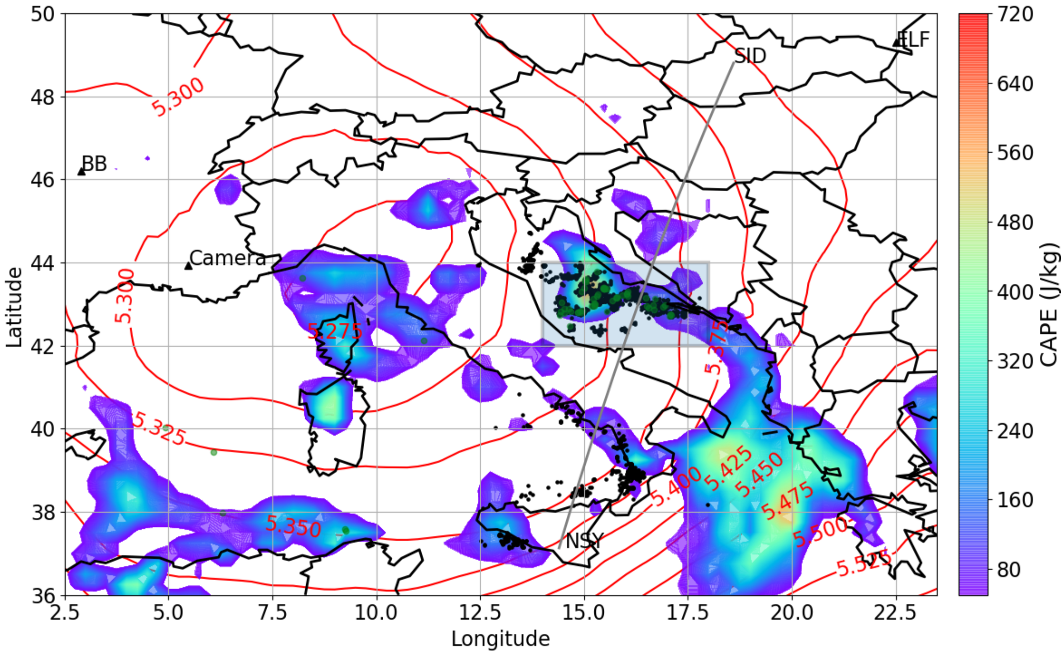

Figure 1. Overview map showing the location of instrumentation used in this study. All CG lightning strokes within ~250 km from the GCP of the VLF signal are plotted in black and the elve producing strokes in green. Red contour lines show the geopotential height at 500 hPa and CAPE is shown in colors. The rectangle frames the region where the elves were observed.

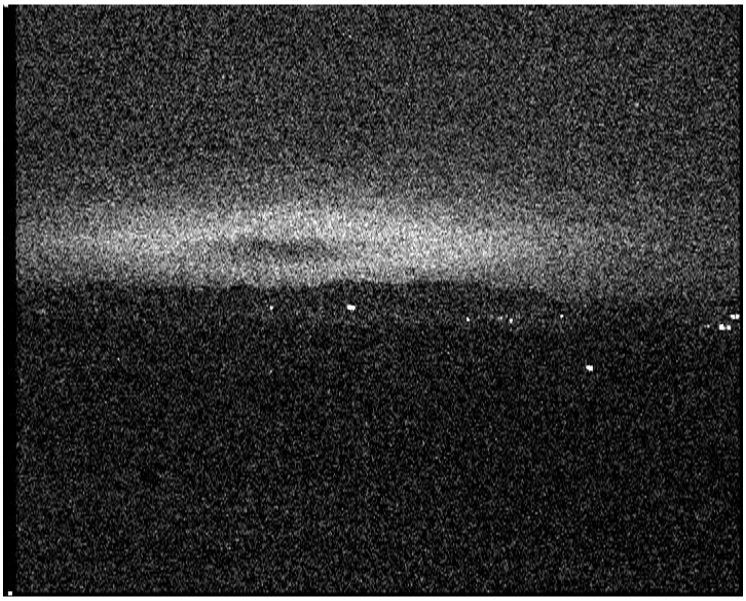

Figure 2. Example of elve image from this study. This elve appeared on December 10 2020, at 03:57:56.578 UTC.

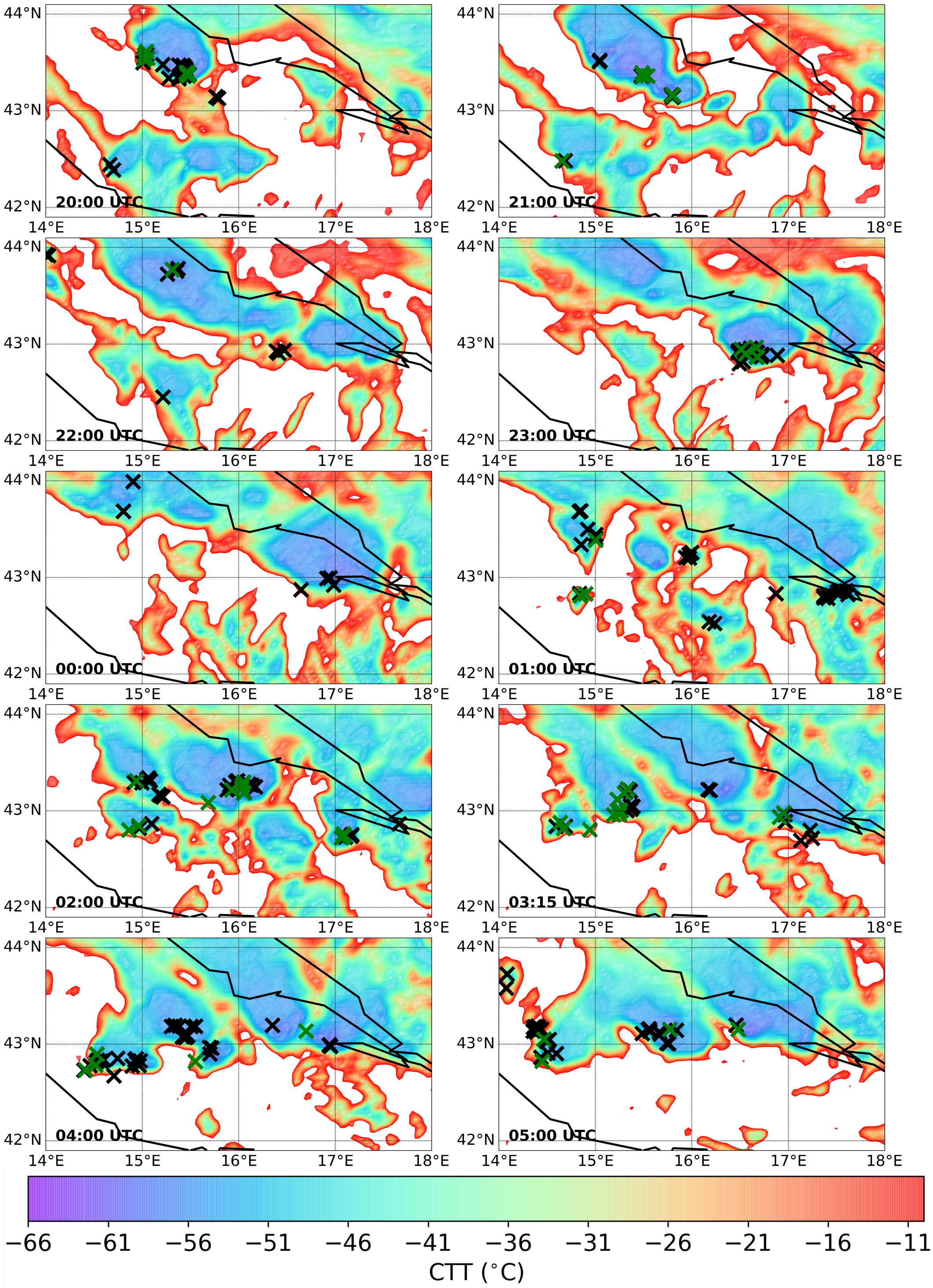

Figure 3. Hourly snapshots of cloud top temperature and strokes with peak currents absolute values higher than 200 kA marked with black crosses from 20 to 05 UTC. The elve-producing strokes are plotted in green.

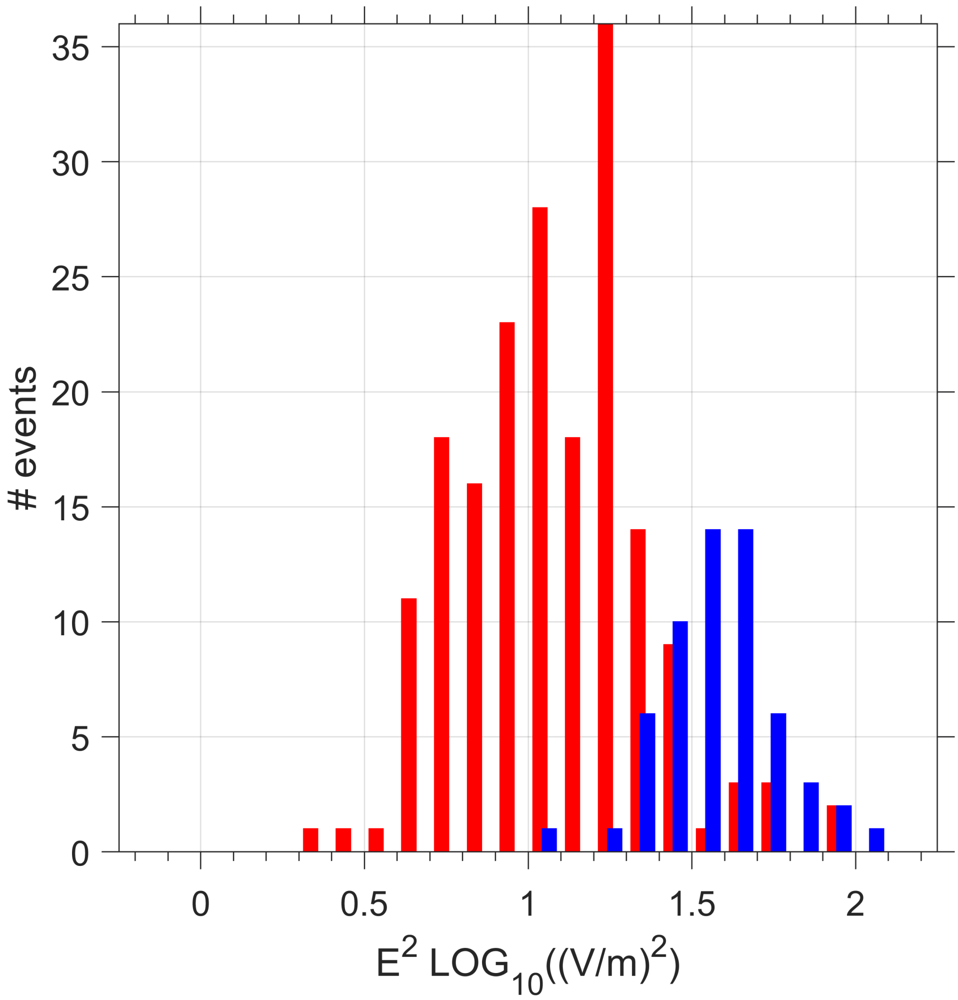

Figure 4. The P(E^2) of the electric field in the band from 1 kHz to 5 MHz computed over 1.5 ms.

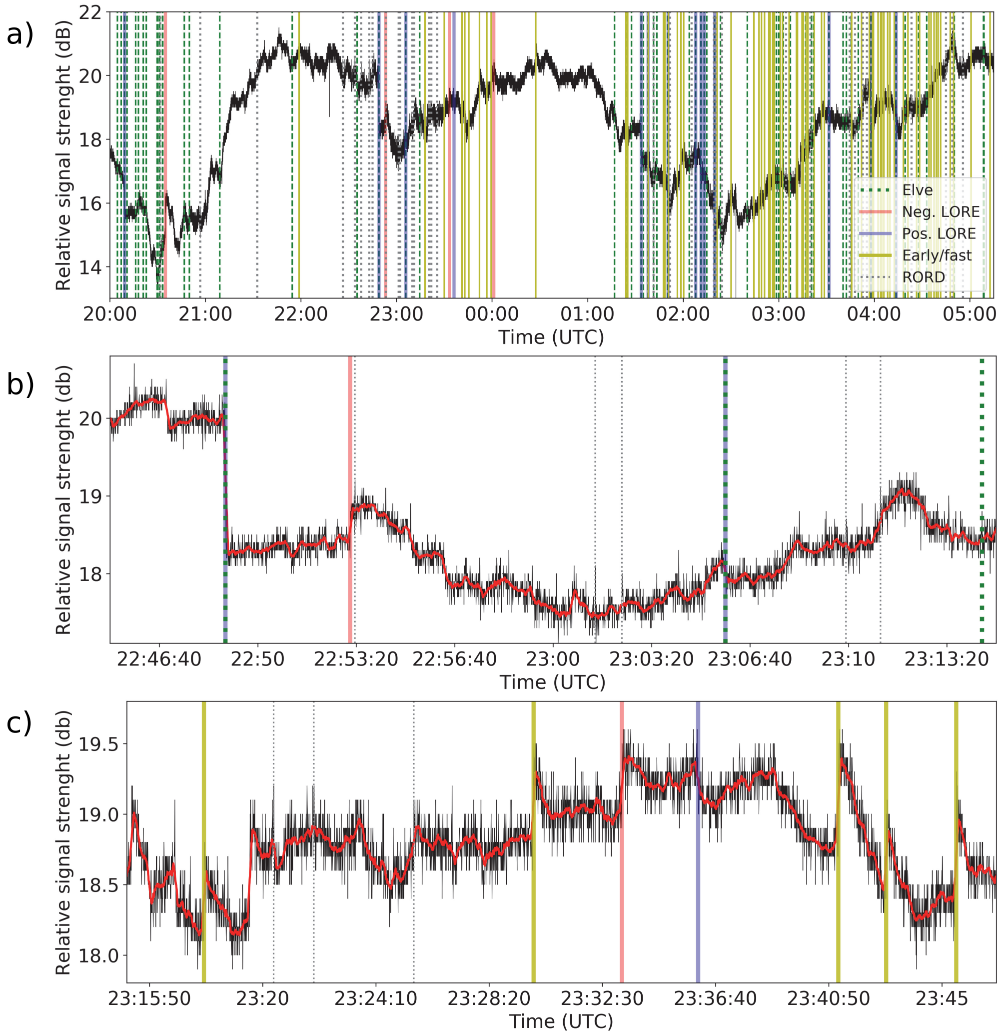

Figure 5. (a) Intensity of the NSY VLF signal (45.9 kHz) recorded in Bojnice (Slovakia) on the night of December 9-10, 2020. Overlaid are the times of elves, LOREs, "early" events and RORD events. b) A zoom of the signal in the time 22:45-23:15 UTC. c) A zoom of the signal in the time 23:15-23:47 UTC.

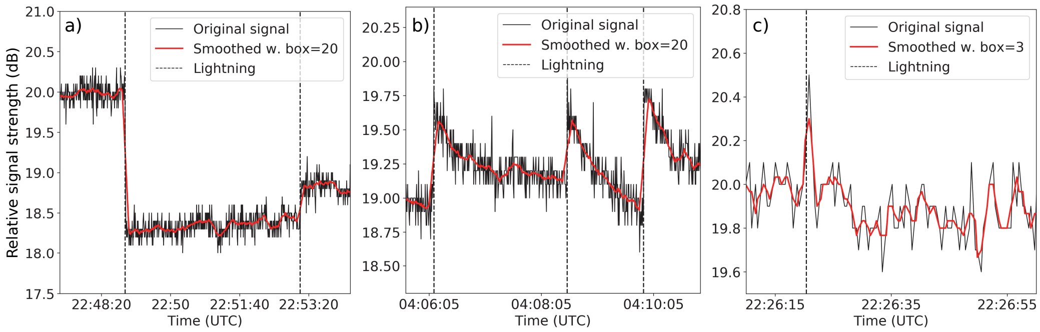

Figure 6. a) An example of a negative and positive LORE event. The negative LORE is caused by a lightning stroke of -725 kA that also produced an elve. The positive LORE is caused by a -530 kA stroke which would likely produce an elve, but the camera was not pointed towards its direction. b) Three examples of "early" events. The first and third have simultaneous strokes with -121 kA and +59 kA currents. The second has no identified stroke but coincides with an IC pulse of -7 kA. c) An example of a RORD event caused by a -155 kA stroke.

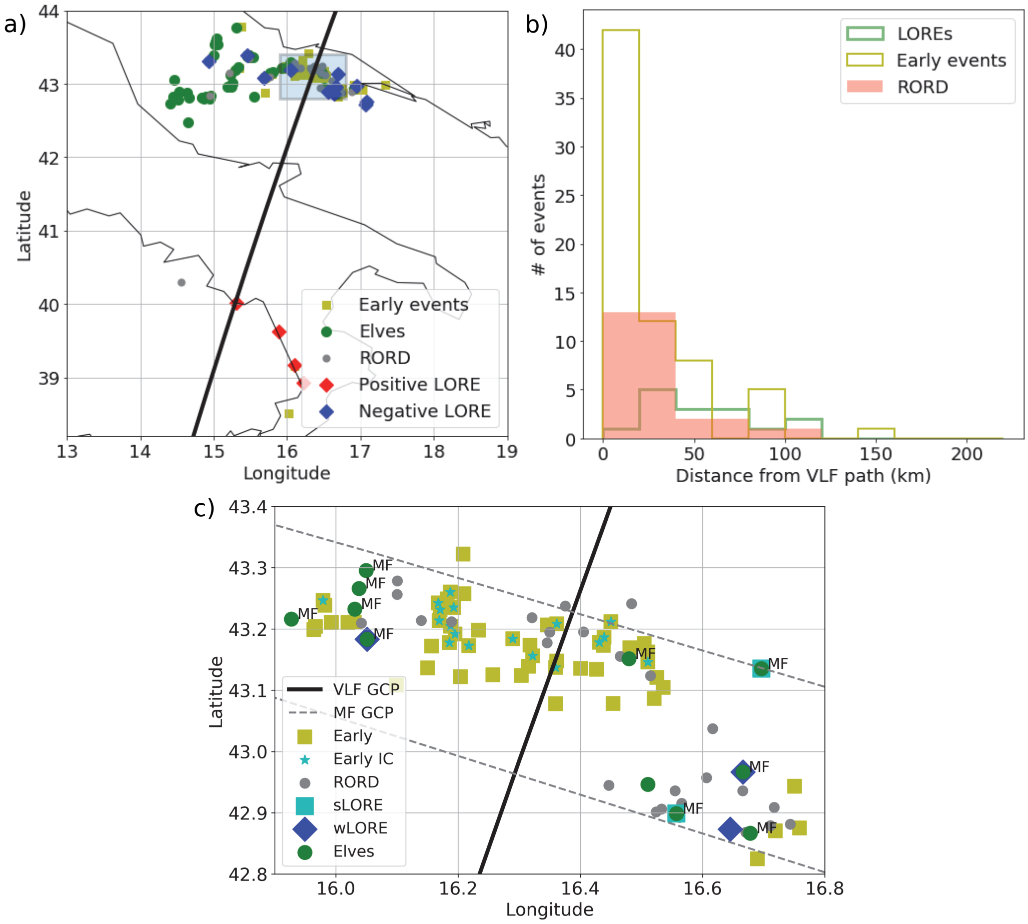

Figure 7. a) Locations of elve-producing strokes (green dots) and LORE-producing strokes (blue/red diamonds). The CG strokes responsible for "early" events are shown with yellow squares and RORD with gray circles. The VLF GCP is shown in black. b) Histogram showing the distance between causative lightning stroke and VLF GCP for the three types of events. c) Zoom to the region marked with a rectangle in panel a). In addition to the markers in panel a), we highlight the strong LOREs (>1 dB) with cyan marker, the "early" events produced by IC pulses with cyan stars and annotate MF blackouts related to an elve. Gray dashed lines are MF GCPs that cross this region.

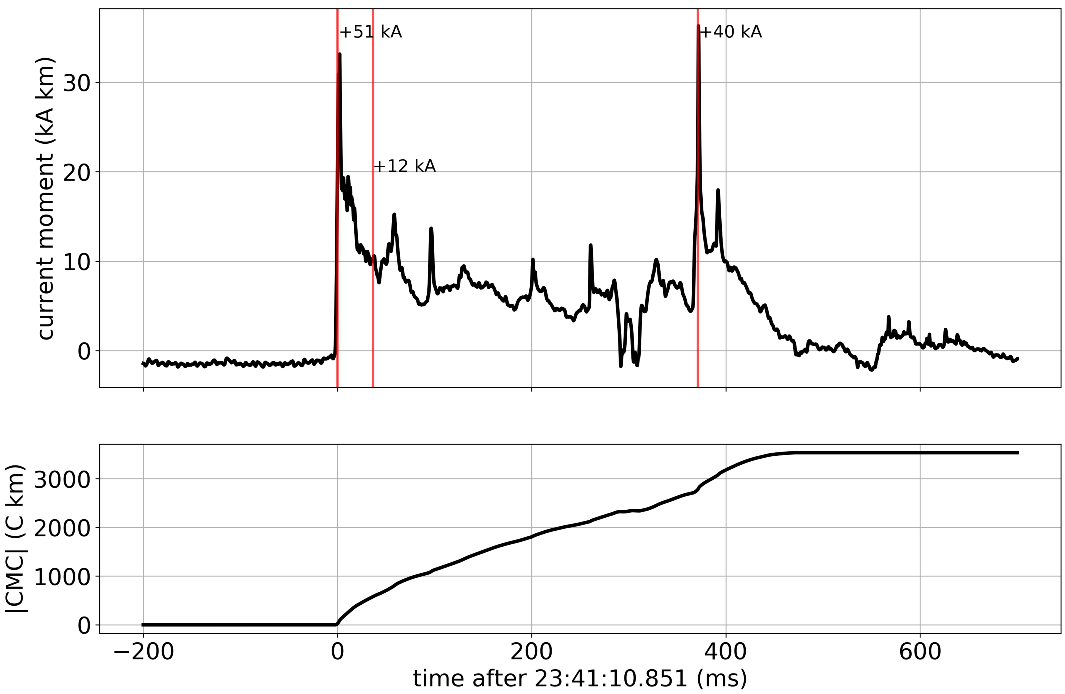

Figure 8. Current moment and charge moment change for "early" event c. The three CG strokes are detected by GLD360.

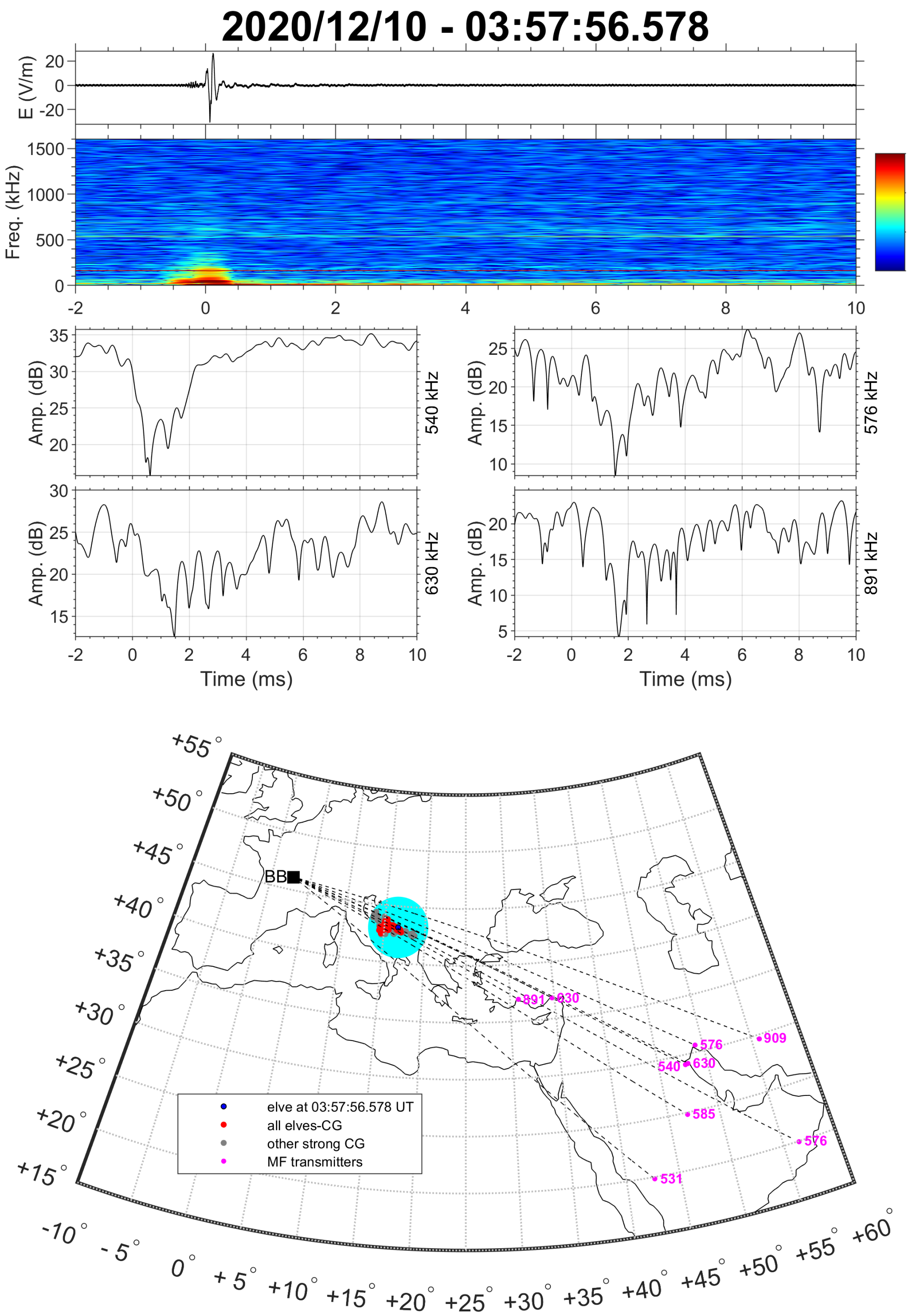

Figure 9. (top) Electric field and associate spectrogram for the elve observed at 03:57:56.578 UTC (shown in Figure 2). (middle): relative amplitude of four transmissions at 540, 576, 630 and 891 kHz (dB). (bottom): map showing the location of the strong CG strokes occurring during the December 9 to 10, 2020 over the Adriatic Sea (grey circles without elves, red ones with elves, the blue circle is for the elve at 03:57:56.578 UT and the light blue disk indicates where the elve is theoretically expanding), magenta dots show the location of transmitters used in this study and the dashed curves are the GCPs of each of these transmitters to the CEA station located in the center of France.

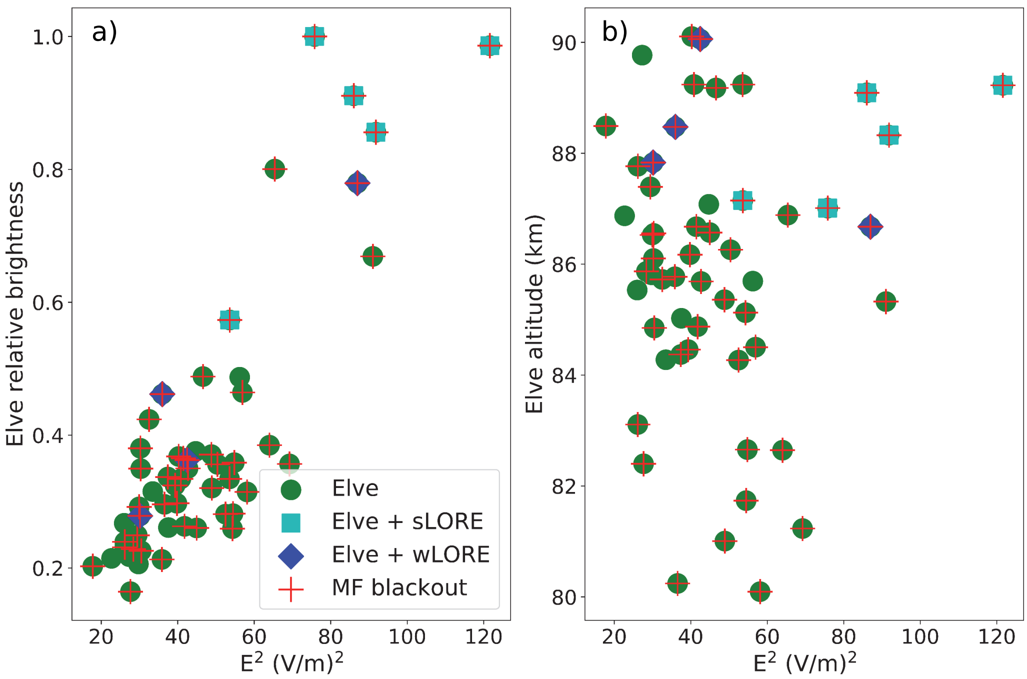

Figure 10. a) Elve relative brightness vs. stroke P(E^2) calculated over 1.5 ms. The elves associated with LOREs and MF blackouts are marked. b) Elve altitude vs. stroke P(E^2) calculated over 1.5 ms. The uncertainty on the altitude is ±1.7 km.

Supporting Information for "Observations of elves and radio wave perturbations by lightning"

Maja Tomicic[1], Olivier Chanrion[1], Thomas Farges[2], Janusz Mlynarczyk[3],

Ivana Kolmašová[4,5], Serge Soula[6], Christoph Köhn[1], Torsten Neubert[1]

[1]DTU Space, Technical University of Denmark, Lyngby, Denmark

[4]Department of Space Physics, Institute of Atmospheric Physics, Czech Academy of Sciences, Prague, Czech Republic

[5]Faculty of Mathematics and Physics, Charles University, Prague, Czech Republic

[2]CEA, DAM, DIF, F-91297, Arpajon, France

[3]Institute of Electronics, AGH University of Science and Technology, Krakow, Poland

[6]Laboratoire d'Aérologie, Université de Toulouse, UT3, CNRS, IRD, Toulouse, France

Contents of this file

Introduction

The Figures S1 to S63 show the background subtracted elve images taken with a Watec 1/2" monochrome CCD camera (WAT-902H) with a 16 mm lens from LSBB in Rustrel. Many of the images have diagonal lines across them. This is an artifact of unknown origin (could be external, such as an radio signal) that we could not remove during post processing of the images because it moved from field to field.

Figure S1. Elve occurring at 2020-12-09T20:04:46.607 UTC.

Figure S2. Elve occurring at 2020-12-09T20:07:07.313 UTC.

Figure S3. Elve occurring at 2020-12-09T20:09:08.216 UTC.

Figure S4. Elve occurring at 2020-12-09T20:10:47.929 UTC.

Figure S5. Elve occurring at 2020-12-09T20:16:13.883 UTC.

Figure S6. Elve occurring at 2020-12-09T20:17:57.214 UTC.

Figure S7. Elve occurring at 2020-12-09T20:20:58.790 UTC.

Figure S8. Elve occurring at 2020-12-09T20:22:55.682 UTC.

Figure S9. Elve occurring at 2020-12-09T20:29:45.575 UTC.

Figure S10. Elve occurring at 2020-12-09T20:29:58.690 UTC.

Figure S11. Elve occurring at 2020-12-09T20:30:08.119 UTC.

Figure S12. Elve occurring at 2020-12-09T20:31:17.727 UTC.

Figure S13. Elve occurring at 2020-12-09T20:32:58.789 UTC.

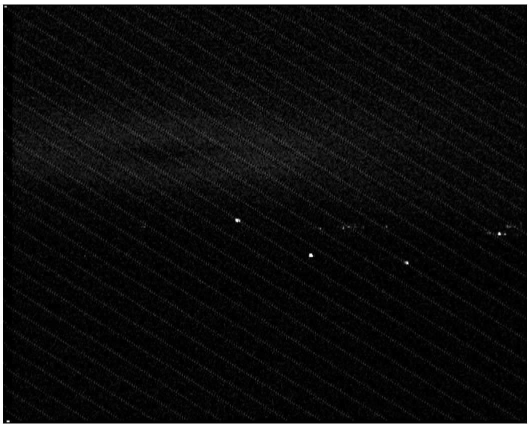

Figure S14. Elve occurring at 2020-12-09T20:33:10.516 UTC.

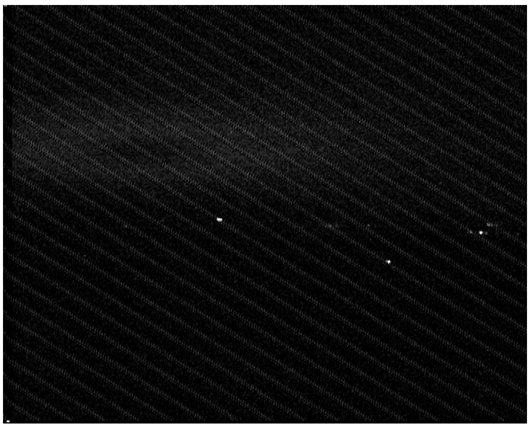

Figure S15. Elve occurring at 2020-12-09T20:46:42.528 UTC.

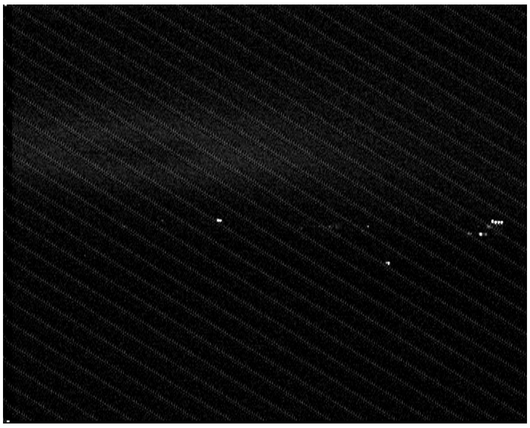

Figure S16. Elve occurring at 2020-12-09T20:49:54.100 UTC.

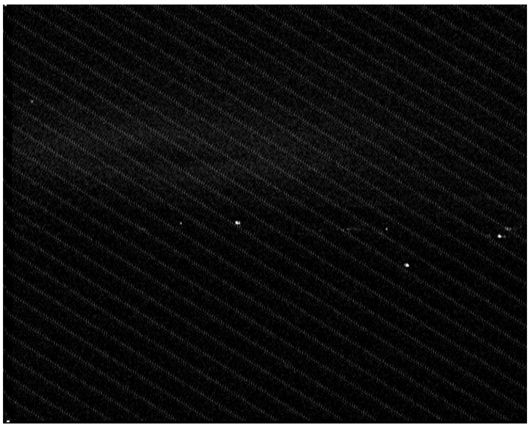

Figure S17. Elve occurring at 2020-12-09T21:09:03.613 UTC.

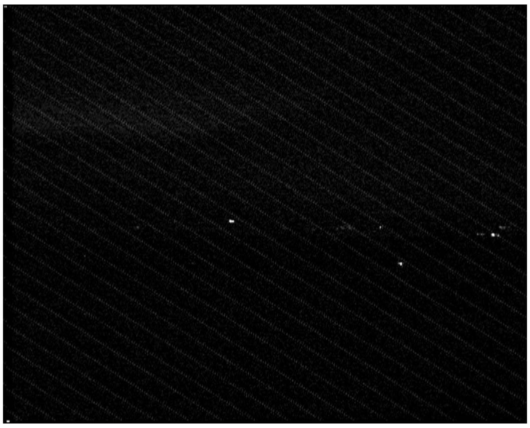

Figure S18. Elve occurring at 2020-12-09T21:54:33.415 UTC.

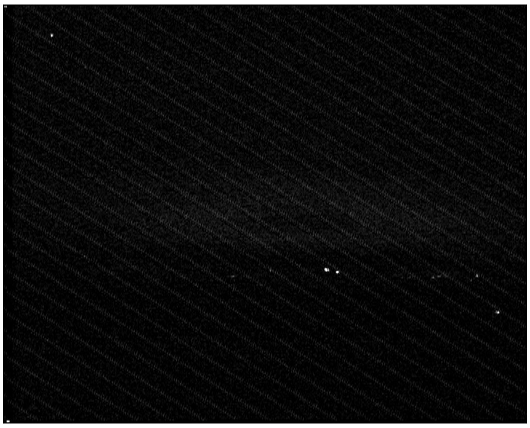

Figure S19. Elve occurring at 2020-12-09T22:35:15.984 UTC.

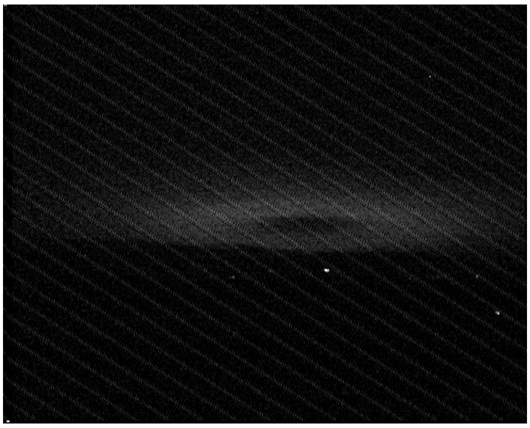

Figure S20. Elve occurring at 2020-12-09T22:48:54.352 UTC.

Figure S21. Elve occurring at 2020-12-09T23:05:50.075 UTC.

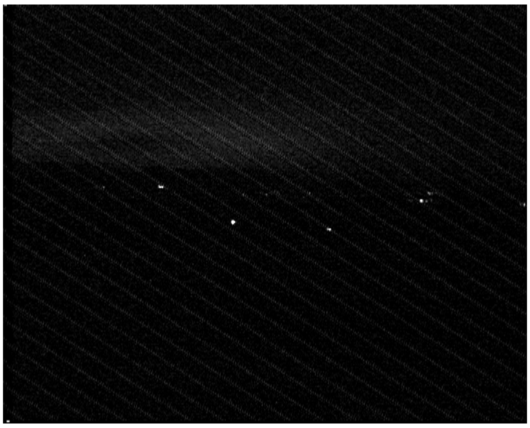

Figure S22. Elve occurring at 2020-12-09T23:14:30.984112607Z UTC.

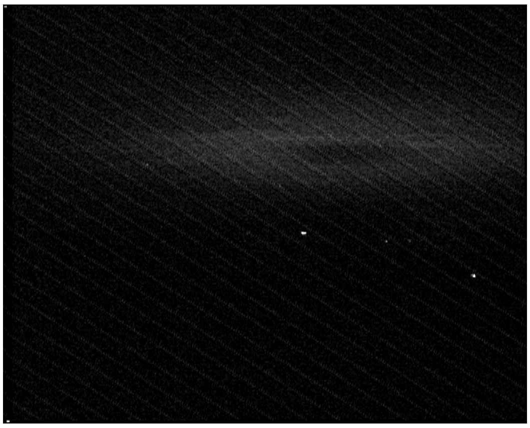

Figure S23. Elve occurring at 2020-12-10T01:16:58.560 UTC.

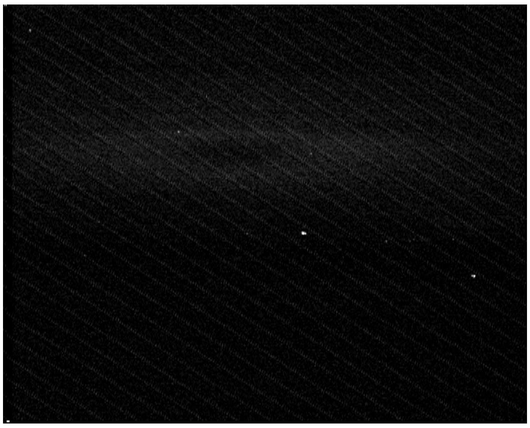

Figure S24. Elve occurring at 2020-12-10T01:24:50.840 UTC.

Figure S25. Elve occurring at 2020-12-10T01:27:34.330 UTC.

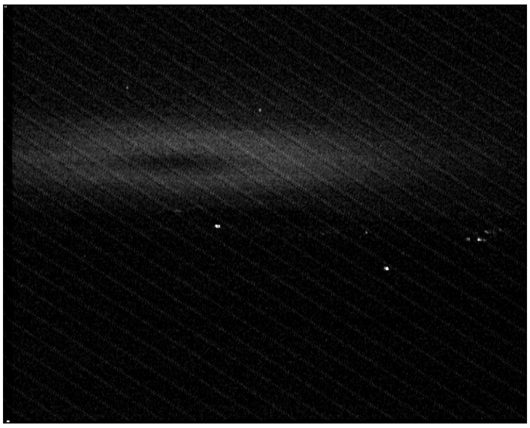

Figure S26. Elve occurring at 2020-12-10T01:33:38.668 UTC.

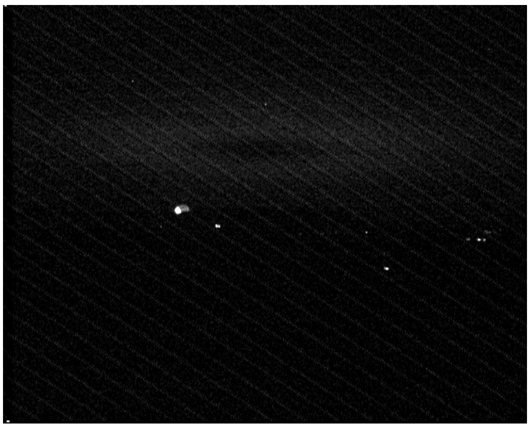

Figure S27. Elve occurring at 2020-12-10T01:35:02.158 UTC.

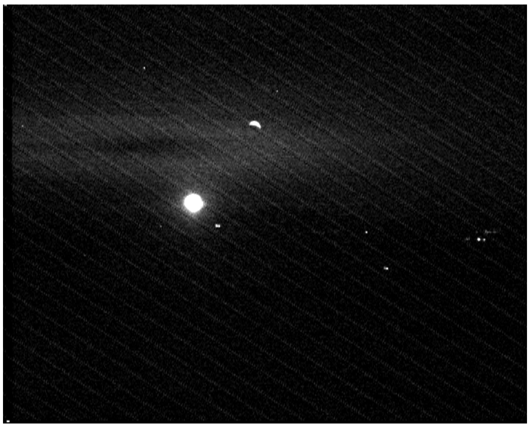

Figure S28. Elve occurring at 2020-12-10T01:37:55.356 UTC.

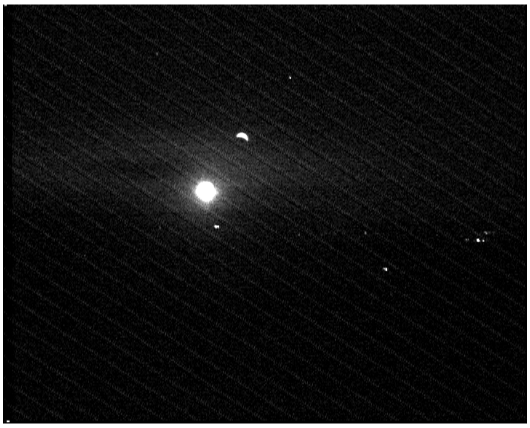

Figure S29. Elve occurring at 2020-12-10T01:41:23.277 UTC.

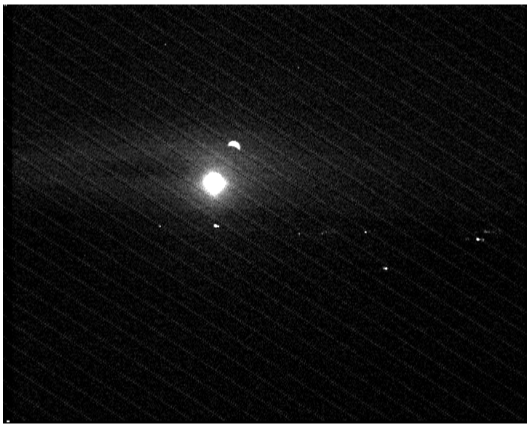

Figure S30. Elve occurring at 2020-12-10T01:43:29.316 UTC.

Figure S31. Elve occurring at 2020-12-10T01:50:15.490 UTC.

Figure S32. Elve occurring at 2020-12-10T01:50:28.950 UTC.

Figure S33. Elve occurring at 2020-12-10T02:03:58.538 UTC.

Figure S34. Elve occurring at 2020-12-10T02:07:50.666 UTC. No CG was detected by GLD360.

Figure S35. Elve occurring at 2020-12-10T02:11:08.862 UTC. No CG was detected by GLD360.

Figure S36. Elve occurring at 2020-12-10T02:13:20.216 UTC.

Figure S37. Elve occurring at 2020-12-10T02:14:48.433 UTC.

Figure S38. Elve occurring at 2020-12-10T02:19:51.788 UTC.

Figure S39. Elve occurring at 2020-12-10T02:23:26.815 UTC.

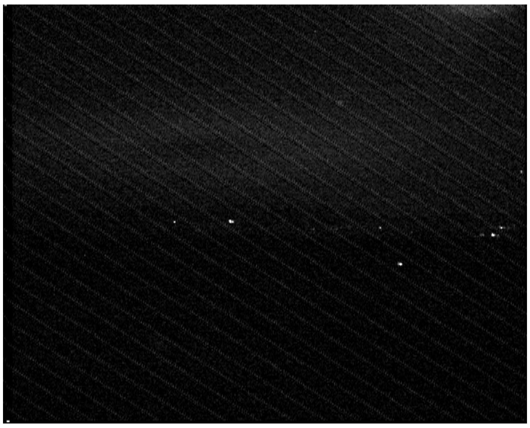

Figure S40. Elve occurring at 2020-12-10T02:40:18.292 UTC.

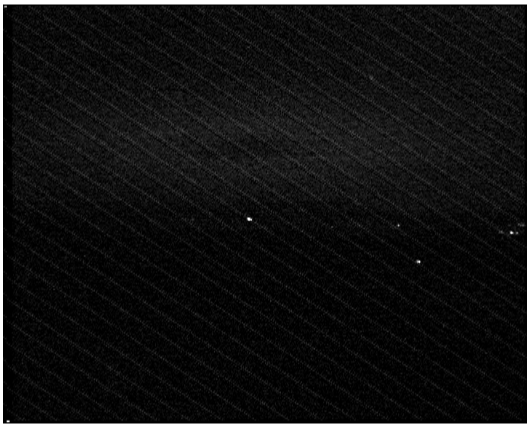

Figure S41. Elve occurring at 2020-12-10T02:54:33.503 UTC.

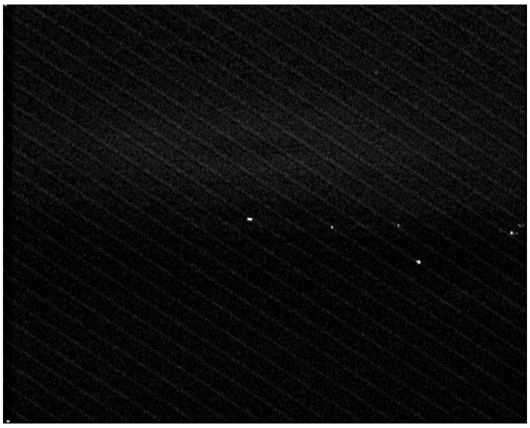

Figure S42. Elve occurring at 2020-12-10T02:57:19.244 UTC.

Figure S43. Elve occurring at 2020-12-10T02:58:34.754 UTC.

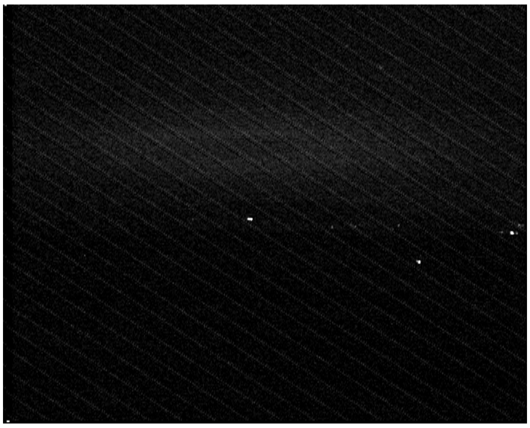

Figure S44. Elve occurring at 2020-12-10T03:00:01.679 UTC.

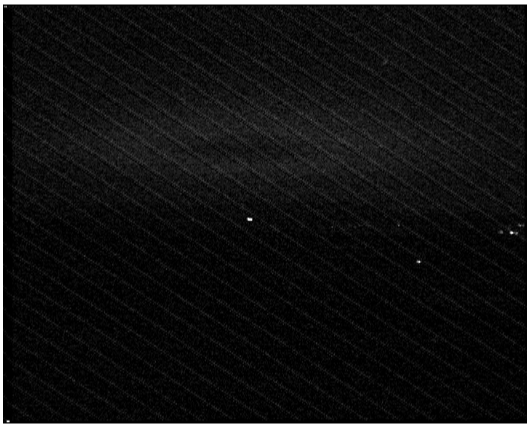

Figure S45. Elve occurring at 2020-12-10T03:02:59.548 UTC.

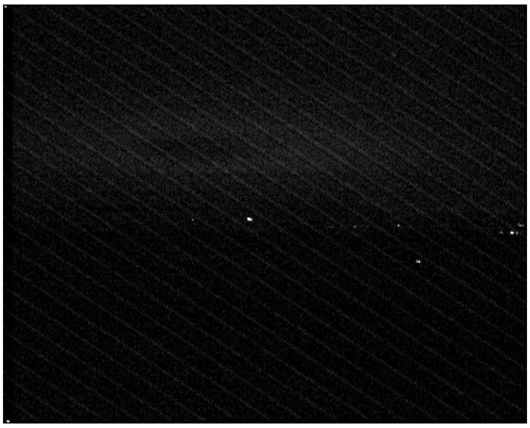

Figure S46. Elve occurring at 2020-12-10T03:07:26.771 UTC.

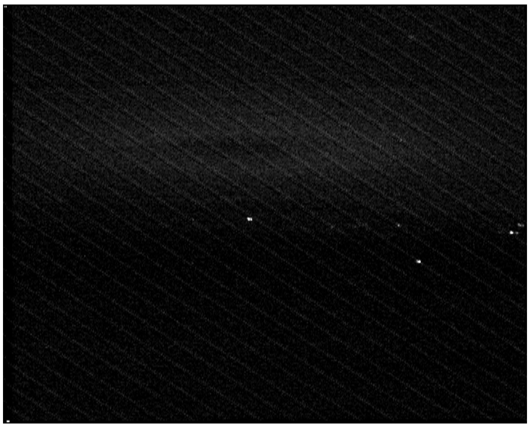

Figure S47. Elve occurring at 2020-12-10T03:16:56.367 UTC.

Figure S48. Elve occurring at 2020-12-10T03:20:33.680 UTC.

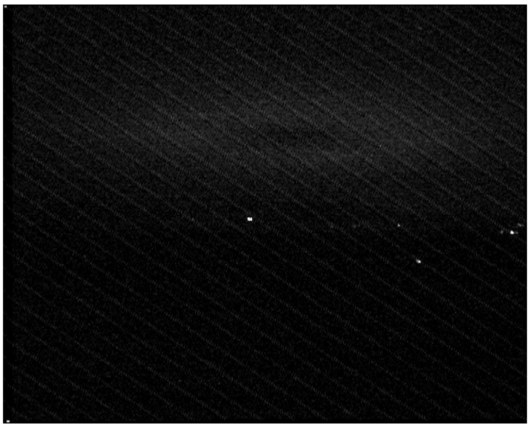

Figure S49. Elve occurring at 2020-12-10T03:21:49.979 UTC.

Figure S50. Elve occurring at 2020-12-10T03:31:32.347 UTC.

Figure S51. Elve occurring at 2020-12-10T03:40:26.663 UTC.

Figure S52. Elve occurring at 2020-12-10T03:42:34.366 UTC.

Figure S53. Elve occurring at 2020-12-10T03:45:38.110 UTC. No CG was detected by GLD360.

Figure S54. Elve occurring at 2020-12-10T03:50:04.616 UTC.

Figure S55. Elve occurring at 2020-12-10T03:57:37.617 UTC.

Figure S56. Elve occurring at 2020-12-10T03:57:56.574 UTC.

Figure S57. Elve occurring at 2020-12-10T04:13:43.939Z UTC. No CG stroke was detected by GLD360.

Figure S58. Elve occurring at 2020-12-10T04:19:28.843 UTC.

Figure S59. Elve occurring at 2020-12-10T04:27:56.658 UTC.

Figure S60. Elve occurring at 2020-12-10T04:33:03.529 UTC.

Figure S61. Elve occurring at 2020-12-10T04:50:20.225 UTC.

Figure S62. Elve occurring at 2020-12-10T05:08:41.960 UTC.

Figure S63. Elve occurring at 2020-12-10T05:09:00.625 UTC.

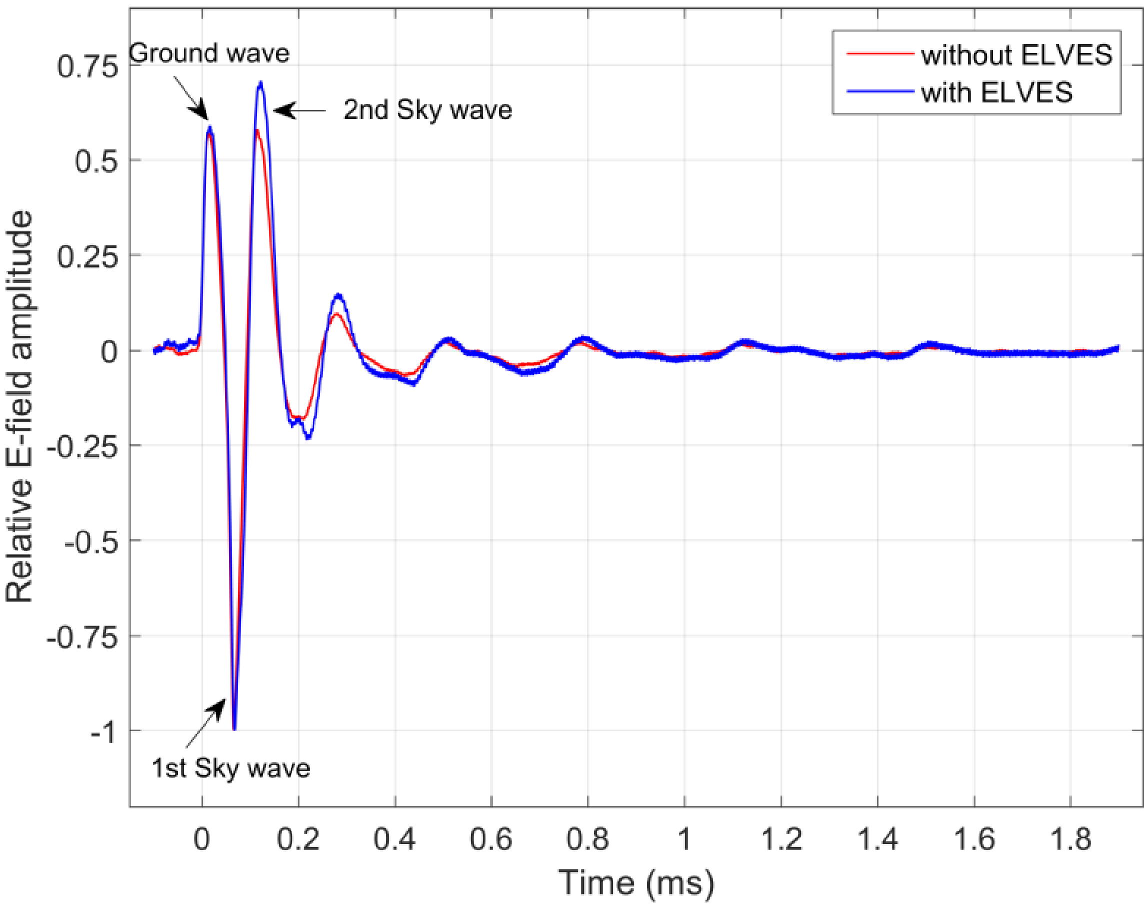

Figure S64. Comparison of stack of normalized waveforms for elve parent strokes (blue) and for not producing elves strokes (red). The ground wave and the first and second sky waves are indicated with arrows. The PSD of each flash (Figure 4 in the paper) is computed over this time window.